Journal of Theoretical Biology ∎ (∎∎∎∎) ∎∎∎–∎∎∎

Contents lists available at ScienceDirect

Journal of Theoretical Biology

journal homepage: www.elsevier.com/locate/yjtbi

Minimal model for human ventricular action potentials in tissue

Alfonso Bueno-Orovio [a], Elizabeth M. Cherry [b,c], Flavio H. Fenton [b,d,*]

[a] Departamento de Matemáticas, Universidad de Castilla-La Mancha, Ciudad Real, Spain
[b] Department of Biomedical Sciences, College of Veterinary Medicine, Cornell University, Ithaca, NY 14853, USA
[c] Department of Physics and Astronomy, Hofstra University, Hempstead, NY 11549, USA
[d] The Heart Institute, Beth Israel Medical Center, New York, NY 10003, USA

ARTICLE INFO

Article history:
Received 10 December 2007
Received in revised form
25 March 2008
Accepted 26 March 2008

PACS:
87.17.Aa
87.18.Hf
87.18.Nq
87.19.Hh

Keywords:
Human ventricular cell modeling
Restitution properties
Spiral waves
Computer simulation
Reentrant arrhythmias

ABSTRACT

Modeling the dynamics of wave propagation in human ventricular tissue and studying wave stability require models that reproduce realistic characteristics in tissue. We present a minimal ventricular (MV) human model that is designed to reproduce important tissue-level characteristics of epicardial, endocardial and midmyocardial cells, including action potential (AP) amplitudes and morphologies, upstroke velocities, steady-state action potential duration (APD) and conduction velocity (CV) restitution curves, minimum APD, and minimum diastolic interval. The model is then compared with three previously published human ventricular cell models, the Priebe and Beuckelmann (PB), the Ten Tusscher–Noble–Noble–Panfilov (TNNP), and the Iyer–Mazhari–Winslow (IMW). For the first time, the stability of reentrant waves for all four models is analyzed, and quantitative comparisons are made among the models in single cells and in tissue. The PB, TNNP, and IMW models exhibit quantitative differences in APD and CV rate adaptation, as well as completely different reentrant wave dynamics of quasi-breakup, stability, and breakup, respectively. All the models have dominant frequencies comparable to clinical values except for the IMW model, which has a large range of frequencies extending beyond the clinical range for both ventricular tachycardia (VT) and ventricular fibrillation (VF). The TNNP and IMW models possess a large degree of short-term memory and we show for the first time the existence of memory in CV restitution. The MV model also can be fitted to reproduce the dynamics of other models and is computationally more efficient: the times required to simulate the MV, TNNP, PB and IMW models follow the ratio 1:31:50:8084.

1. Introduction

Modeling the dynamics of wave propagation in human ventricular tissue and studying the stability of reentrant waves and their relation to arrhythmias require the use of ionic models that not only reproduce key characteristics such as the rate dependence of action potential duration (APD), but also tissue-level characteristics that are important for describing correct wave propagation and dynamics. These properties include upstroke rate of rise, wavefront curvature, and the minimum rate before conduction block, all of which are observed not in isolated cells but only in tissue. In addition, it is important to reproduce action potential (AP) morphologies accurately in tissue because it is known that electrotonic currents modify the APs produced by isolated cells, potentially altering the AP amplitude and affecting the relationships among the transmembrane currents (Cherry and Fenton, 2007). Properly reproducing tissue-level characteristics is important because they have been shown to affect the initiation, dynamics, and stability of reentrant waves (Cherry and Fenton, 2004, 2007; Ten Tusscher and Panfilov, 2006a).

In addition to reproducing electrophysiological properties accurately, the most useful tissue-level models should possess several other characteristics. First, it is desirable for a model to be easily configured to reproduce these experimentally measured tissue characteristics from various regions of normal and diseased cardiac tissue, to facilitate matching experimentally observed spatial variations in properties. Second, computational efficiency of the model is key to being able to perform large-scale simulations, especially using detailed three-dimensional (3D) anatomies with fiber anisotropy at an adequate spatial resolution. Finally, a model should retain enough complexity to reproduce tissue behavior accurately while remaining simple enough to gain insights into the parameters responsible for its observed behavior.

To date, three different ionic models have been developed to reproduce human ventricular cell dynamics. First, the

---

[*] Corresponding author at: Department of Biomedical Sciences, College of Veterinary Medicine, Cornell University, Ithaca, NY 14853, USA.
Tel.: +1 607 253 3075; fax: +1 607 253 3851.
E-mail address: fhf3@cornell.edu (F.H. Fenton).

0022-5193/$ - see front matter © 2008 Elsevier Ltd. All rights reserved.
doi:10.1016/j.jtbi.2008.03.029

Please cite this article as: Bueno-Orovio, A., et al., Minimal model for human ventricular action potentials in tissue. J. Theor. Biol. (2008), doi:10.1016/j.jtbi.2008.03.029

Priebe–Beuckelmann (PB) model (Priebe and Beuckelmann, 1998), which consists of 22 variables, was developed to study the cellular electrophysiological consequences of heart failure and abnormal automaticity and was derived from the LR-II model with five of the ionic currents based on experiments in human myocytes. A simplified 6-variable version of this model, the Bernus–Wilders–Zemlin–Verschelde–Panfilov (BWZVP) model, was developed later for normal epicardial, endocardial, and midmyocardial cells (Bernus et al., 2002a). Second, the Ten Tusscher–Noble–Noble–Panfilov (TNNP) model (Ten Tusscher et al., 2004) consists of 17 variables and used new formulations for most of the major ionic currents based on experiments in human ventricular myocytes and ion channel expressions. Third, the Iyer–Mazhari–Winslow (IMW) model (Iyer et al., 2004) consists of 67 variables and is based on data from human myocytes and recombinant human ion channels. In contrast to the PB and TNNP models, which use Hodgkin–Huxley-type equations, the IMW model uses Markov chains to model the dynamics of all but one of its ion channel gates.

The purpose of this manuscript is twofold. First, it introduces a model, which we call the minimal model, that reproduces in detail experimentally measured characteristics of human ventricular APs in isolated cells and in tissue while improving computational tractability and increasing the flexibility to incorporate variations compared to previous models. Second, it presents for the first time a quantitative comparison in tissue of the electrophysiological and dynamical properties of the three previously developed models and the minimal model, including the behavior of reentrant waves they generate in two dimensions.

2. Methods

2.1. Model development and implementation

Using previously published data (Morgan et al., 1992; Sakakibara et al., 1993; Drouin et al., 1995, 1998; Nabauer et al., 1996; Li et al., 1998; Pereon et al., 2000; Pak et al., 2004; Koller et al., 2005), we developed a minimal model of the APs of human ventricular myocytes, where resting membrane potential, threshold for excitation, upstroke, AP morphology, and APD and conduction velocity (CV) rate dependence were fitted. The model is based on the three-variable model proposed by Fenton and Karma (1998). Although this three-variable formulation is sufficient to reproduce arbitrary APD and CV restitution curves, it is not possible to reproduce AP shapes accurately, especially spike-and-dome morphologies. Therefore, a fourth variable has been added (Fenton, 1999) to adjust the inward current in order to obtain an accurate AP morphology, as AP shape can have an important role in dynamics, especially during alternans (Fenton, 2000; Cherry and Fenton, 2004; Ten Tusscher and Panfilov, 2006a). The resulting four-variable model is referred to as the minimal ventricular (MV) model, as it contains the minimum number of variables necessary for an AP model that can reproduce arbitrary APD and CV restitution curves as well as a range of realistic AP shapes. The differential equations for the four variables are as follows:

$$
\begin{aligned}
\partial_t u &= \nabla(\tilde{D}\nabla u) - (J_{fi} + J_{so} + J_{si})\\
\partial_t v &= (1 - H(u - \theta_v))(v_\infty - v)/\tau_v^- - H(u - \theta_v)v/\tau_v^+\\
\partial_t w &= (1 - H(u - \theta_w))(w_\infty - w)/\tau_w^- - H(u - \theta_w)w/\tau_w^+\\
\partial_t s &= ((1 + \tanh(k_s(u - u_s)))/2 - s)/\tau_s,
\end{aligned}
$$

where the three currents are given by the following equations:

$$
\begin{aligned}
J_{fi} &= -vH(u - \theta_v)(u - \theta_v)(u_u - u)/\tau_{fi}\\
J_{so} &= (u - u_o)(1 - H(u - \theta_w))/\tau_o + H(u - \theta_w)/\tau_{so}\\
J_{si} &= -H(u - \theta_w)ws/\tau_{si}
\end{aligned}
$$

and $H(x)$ is the standard Heaviside function. Several time constants are functions of the voltage variable u and are defined as follows:

$$
\begin{aligned}
\tau_v^- &= (1 - H(u - \theta_v^-))\tau_{v1}^- + H(u - \theta_v^-)\tau_{v2}^-\\
\tau_w^- &= \tau_{w1}^- + (\tau_{w2}^- - \tau_{w1}^-)(1 + \tanh(k_w^-(u - u_w^-)))/2\\
\tau_{so} &= \tau_{so1} + (\tau_{so2} - \tau_{so1})(1 + \tanh(k_{so}(u - u_{so})))/2\\
\tau_s &= (1 - H(u - \theta_w))\tau_{s1} + H(u - \theta_w)\tau_{s2}\\
\tau_o &= (1 - H(u - \theta_o))\tau_{o1} + H(u - \theta_o)\tau_{o2}
\end{aligned}
$$

and the infinity values are defined as

$$
v_\infty = \begin{cases} 1, & u < \theta_v^- \\ 0, & u \geqslant \theta_v^- \end{cases}
$$

$$
w_\infty = (1 - H(u - \theta_o))(1 - u/\tau_{w\infty}) + H(u - \theta_o)w_\infty^*.
$$

Initial conditions are $u = 0$, $v = 1$, $w = 1$, and $s = 0$. The dimensionless voltage variable u is rescaled to dimensions of mV using the equation $V_{mV} = 85.7u - 84$. Different parameter sets (see Table 1) were developed to reproduce experimentally measured epicardial, endocardial, and midmyocardial cell properties as well as to reproduce the dynamics of two previously developed ionic models for human ventricular cells (Priebe and Beuckelmann, 1998; Ten Tusscher et al., 2004).

This minimal model formulation differs from more complex ionic models in that instead of reproducing a wide range of ion channel currents, it is designed to account for the sum of all the transmembrane currents represented in three main categories: fast inward, slow inward, and outward currents. It has been shown previously that these total currents retain enough structure of the basic currents involved in cardiac excitation to reproduce exact AP morphologies (Fenton, 1999; Fenton et al., 2002a) and are flexible enough that the parameters can be fitted to replicate accurately the properties and dynamics of other complex ionic models as well as experimental data (Fenton and Karma, 1998; Fenton et al., 2002a; Oliver and Krassowska, 2005; Nash et al., 2006), such as

Table 1
Model parameter values

Parameter	EPI	ENDO	M	PB	TNNP
u_o	0	0	0	0	0
u_u	1.55	1.56	1.61	1.45	1.58
θ_v	0.3	0.3	0.3	0.35	0.3
θ_w	0.13	0.13	0.13	0.13	0.015
θ_v^-	0.006	0.2	0.1	0.175	0.015
θ_o	0.006	0.006	0.005	0.006	0.006
τ_{v1}^-	60	75	80	10	60
τ_{v2}^-	1150	10	1.4506	1150	1150
τ_v^+	1.4506	1.4506	1.4506	1.4506	1.4506
τ_{w1}^-	60	6	70	140	70
τ_{w2}^-	15	140	8	6.25	20
k_w^-	65	200	200	65	65
u_w^-	0.03	0.016	0.016	0.015	0.03
τ_w^+	200	280	280	326	280
τ_{fi}	0.11	0.1	0.078	0.105	0.11
τ_{o1}	400	470	410	400	6
τ_{o2}	6	6	7	6	6
τ_{so1}	30.0181	40	91	30.0181	43
τ_{so2}	0.9957	1.2	0.8	0.9957	0.2
k_{so}	2.0458	2	2.1	2.0458	2
u_{so}	0.65	0.65	0.6	0.65	0.65
τ_{s1}	2.7342	2.7342	2.7342	2.7342	2.7342
τ_{s2}	16	2	4	16	3
k_s	2.0994	2.0994	2.0994	2.0994	2.0994
u_s	0.9087	0.9087	0.9087	0.9087	0.9087
τ_{si}	1.8875	2.9013	3.3849	1.8875	2.8723
$\tau_{w\infty}$	0.07	0.0273	0.01	0.175	0.07
w_∞^*	0.94	0.78	0.5	0.9	0.94

Please cite this article as: Bueno-Orovio, A., et al., Minimal model for human ventricular action potentials in tissue. J. Theor. Biol. (2008), doi:10.1016/j.jtbi.2008.03.029

APD and CV restitution curves, thresholds for excitation, upstroke velocities, minimum APDs and diastolic intervals (DIs) before reaching conduction block.

It is important to note that in contrast to some reports (Bernus et al., 2002b; Nash and Panfilov, 2004), this model formulation is not equivalent to FitzHugh–Nagumo-type models, which have the unphysiological characteristic of not producing a minimum DI for propagation, as fronts can be generated at any DI larger than zero (as the ratio of upstroke time to activation time goes to zero). The minimal model does not have a Maxwell point and thus, like other complex ionic models, it has a well-defined minimum diastolic interval for propagation in tissue that can be varied as a function of the parameters describing the sodium channel kinetics, particularly τ_v^-.

Just as the minimal model can be set to reproduce experimental data, it is also possible to choose parameter values to reproduce the behavior of other models. In particular, parameter sets that reproduce the dynamics of the PB and TNNP models are provided along with comparisons to the original models.

2.2. *Parameter fitting*

AP morphologies and other properties were carefully matched in all cases using a parameter-fitting algorithm. By construction, each model parameter has a particular well-characterized effect on the electrophysiological properties, so that it is relatively simple to obtain seed parameter values for each data set based on the desired characteristics (Fenton and Karma, 1998; Fenton, 1999; Oliver and Krassowska, 2005). Examples of properties that can be fitted in a straightforward manner include maximum AP upstroke velocity (controlled primarily by τ_{fi}, τ_v^+, and θ_v), AP amplitude (controlled primarily by u_u and u_o), maximum and minimum APD (controlled primarily by $\tau_w{}^+$, τ_{si}, and τ_{so}), and minimum DI (τ_v^-). The effects of other parameters have been discussed previously (Fenton, 1999; Oliver and Krassowska, 2005). At each iteration step, an error functional is defined as the mean quadratic error between the experimental data and the output for the minimal model. The aim is then to find a constrained minimum (in order to maintain parameters within their range of physiological values) of a scalar function of several variables starting at the initial seed estimate. A sequential quadratic programming (SQP) method is used to solve this constrained nonlinear optimization problem. SQP methods represent the state-of-the-art in nonlinear programming methods, since they guarantee superlinear convergence by accumulating second-order information regarding the necessary conditions for optimality using a quasi-Newton updating procedure. At each major iteration, an approximation of the Hessian of the Lagrangian function is made using a quasi-Newton updating method. This is then used to generate a quadratic programming subproblem whose solution is used to form a search direction for a line search procedure. We refer the reader to selected publications (Fletcher, 1987; Gill et al., 1981) and the example code referenced in Appendix A for more details on the implementation of this type of method.

Because uniqueness of the solution is not guaranteed (different sets of parameters can result in the same shape of the AP waveform), the parameters are further constrained by including data for APD and CV rate dependence, and the error between the experimental data and the output for the minimal model is newly minimized. Both parts of the fitting process are then repeated sequentially until they converge to a single set of final parameter values.

Although gradient-based optimization routines were used, other optimization approaches, like genetic algorithms techniques, were verified to provide similar results. This type of approach has been shown to calculate conductance parameters successfully for arbitrary AP waveforms (Syed et al., 2005).

2.3. *Numerical methods*

All the models were implemented first using an explicit Euler method with uniform spatial and temporal resolution in Fortran with no optimizations of the integration schemes. The method of Rush and Larsen (1978) was used to integrate the gating variables. Then the programs were optimized by tabulating precomputed lookup tables for computationally intensive functions (including exponentials, non-integer powers, and hyperbolic functions) of one variable. In addition, in the optimized IMW code some variables were integrated semi-implicitly to improve numerical stability and accuracy at larger time step intervals. This allowed the use of a time step of 0.01 ms and a spatial discretization of 0.2 mm for all the models (without optimizations, the IMW code requires a time step of 0.00002 ms as in Fink et al. (2006) in order to be numerically stable). To prevent violation of charge conservation that can result in long-term drift in models that include intracellular ion concentrations, the stimulus and electrotonic currents were attributed to K^+ (Hund et al., 2001; Kneller et al., 2002). The accuracy of the numerical simulations for all models was verified in one-dimensional (1D) cables by decreasing the time and space integration steps by a factor of two and verifying that this resulted in a change of less than 5% in their conduction velocities (Bernus et al., 2002a; Ten Tusscher et al., 2004). The diffusion coefficient is calculated specifically for human ventricular tissue from experimental values, as detailed in Appendix A, resulting in a value of $1.171 \pm 0.221\,\mathrm{cm}^2/\mathrm{s}$. In all tissue simulations, no-flux boundary conditions were used. For the 3D simulations used for pseudo-ECG calculations (see Section 2.6), a phase-field method (Fenton et al., 2005; Bueno-Orovio et al., 2006) was used to implement the no-flux boundary conditions in an irregular domain. The 2D and 3D simulations were performed using parallel computers with MPI on a 96-processor cluster and at the Pittsburgh Supercomputing Center.

2.4. *Calculation of APD and CV restitution curves*

The restitution curves of all models were calculated in tissue, using 1D cables 2 cm in length and stimulated at one end with a stimulus of strength twice diastolic threshold. APD restitution was measured in tissue for three reasons: first, to match the experimental data, which was obtained in tissue; second, to avoid sensitive dependence on the stimulus (Fenton et al., 2002a; Vigmond and Leon, 2002; Henry and Rappel, 2005); and third, to obtain the minimum DI for propagation. All $S1$–$S2$ APD restitution curves were measured by pacing at a specified $S1$ cycle length (CL) until steady state was reached or for a maximum of 2500 beats (for the IMW and TNNP models) and then introducing test pulses over a range of intervals. The resulting DI, APD pairs constituted a single $S1$–$S2$ restitution curve. By varying the $S1$ CL used, a family of $S1$–$S2$ restitution curves was generated. Steady-state (also called dynamic) APD restitution curves were obtained from the steady-state values of the various $S1$–$S2$ restitution curves. CV restitution curves were measured from the steady-state restitution protocols between neighboring points located 1 cm along the cable from the site of stimulation. For all restitution curves, linear interpolation was used to calculate APD_{90}.

2.5. *Spiral wave protocols*

Spiral waves were initiated in 2D tissue using a cross-field stimulation protocol in which a planar wave was initiated from

Please cite this article as: Bueno-Orovio, A., et al., Minimal model for human ventricular action potentials in tissue. J. Theor. Biol. (2008), doi:10.1016/j.jtbi.2008.03.029

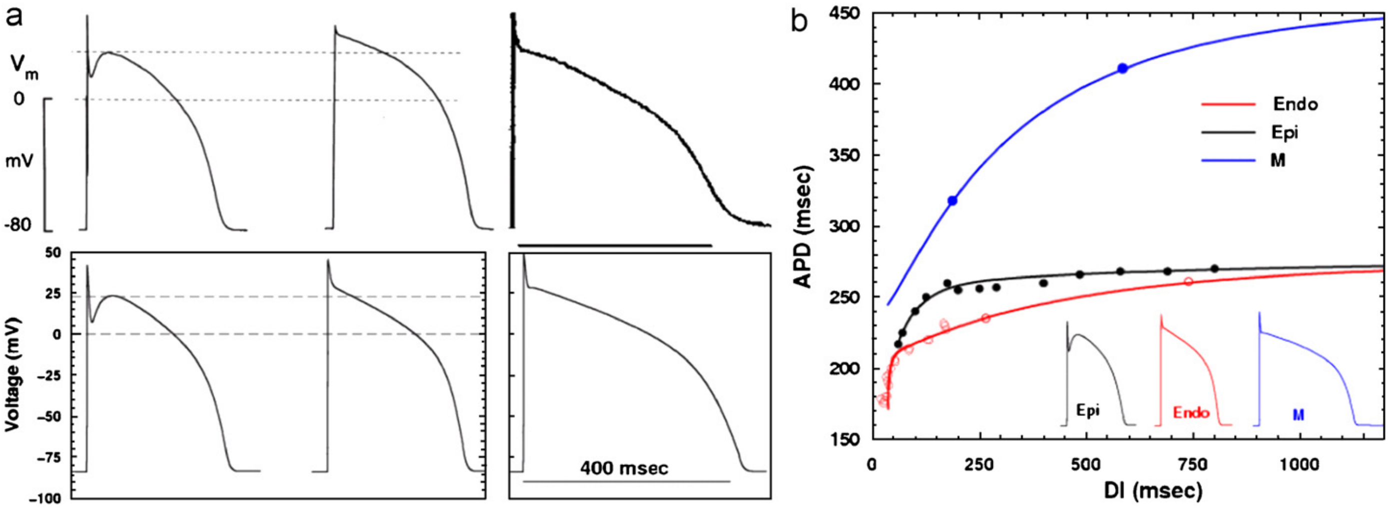

Fig. 1. Experimental and simulated human ventricular action potentials and steady-state restitution curves: (a) Top: experimental epicardial (Nabauer et al., 1996), endocardial (Nabauer et al., 1996), and midmyocardial (Drouin et al., 1995) human ventricular APs. Bottom: simulated epicardial, endocardial, and midmyocardial APs using the MV model. Only the epicardial AP has a prominent spike-and-dome morphology. (b) APD restitution curves include experimental data (circles) and minimal model curves (solid lines), with endocardial data (red) from Drouin et al. (1995), Drouin et al. (1998), and Li et al. (1998); epicardial data (black) as used by Ten Tusscher et al. (2004) from Morgan et al. (1992); and midmyocardial data (blue) that is the average from Drouin et al. (1995) and Li et al. (1998) with the minimal model single cell APs shown below. In the model at long DIs, the endocardial AP is nearly as long as the epicardial, but it becomes much shorter than the epicardial AP at short DIs.

one edge of the tissue and propagated partway across the medium before being disrupted by a second stimulus applied to a different region of the tissue, thereby generating a spiral wave. Tissue sizes used were large enough to prevent the boundaries from modifying spiral wave dynamics. Spiral tip trajectories were computed using the zero-normal-velocity method (Fenton and Karma, 1998). Period distributions or period spectra were obtained by calculating the intervals between activations for all grid points in the 2D domain during the entire spiral wave simulation and then normalizing to the maximum value.

2.6. Pseudo-ECG calculation

Pseudo-ECGs were calculated using a digitized 3D piece of porcine left ventricular free wall (Stevens et al., 2003). The distribution of cell layers across the ventricle was chosen to be approximately 20% epicardial cells, 50% endocardial cells and the rest midmyocardial cells, roughly matching the experimental values of Drouin et al. (1995). The transmural pseudo-ECGs were obtained by assuming an infinite volume conductor and calculating the dipole source density of the membrane potential V in all node points of the medium using the equation $\mathrm{ECG} = \int (D\nabla V r/r^3)\,\mathrm{d}x$, where r is the vector from the recording electrode to a point in the tissue. The recording electrode was placed 0.5 cm away from the center of the epicardial surface of the preparation. Note that the pseudo-ECG is a function of the recording electrode position and stimulation site (Clayton and Holden, 2002).

3. Results

3.1. Minimal model properties

Using experimental data (Morgan et al., 1992; Sakakibara et al., 1993; Drouin et al., 1995, 1998; Nabauer et al., 1996; Li et al., 1998; Pereon et al., 2000; Pak et al., 2004; Koller et al., 2005), three parameter sets were developed (see Appendix A) for the minimal model as described in the Methods section to reproduce epicardial, endocardial, and midmyocardial AP morphologies (Fig. 1a), APD rate of adaptation (Fig. 1b), and other important electrophysiological characteristics, described below and summarized in Table 2.

The epicardial model in tissue has a $\mathrm{d}v/\mathrm{d}t_{max}$ of 227 V/s, which matches the experimental value of 228 ± 11 V/s from Drouin et al. (1995) and is also close to the measurement of 196 ± 20 V/s from Pereon et al. (2000). Its phase 0 amplitude is 122 mV, compared to 123 mV (Nabauer et al., 1996) and 131 mV (Li et al., 1998). The minimum voltage of the AP notch is 7 mV, compared to 8.6 mV (Nabauer et al., 1996) and 9 mV (Li et al., 1998), and its plateau voltage (where $\mathrm{d}^2v/\mathrm{d}t^2 = 0$) occurs at 23 mV, the same value as shown experimentally (Nabauer et al., 1996; Li et al., 1998). APD_{90} at 1 Hz is 269 ms, comparable to the experimental value of 271 ± 13 ms obtained by Li et al. (1998). The steady-state APD restitution curve was calculated to fit the experimental APD values of Morgan et al. (1992) (which were also used for the TNNP model (Ten Tusscher et al., 2004)), shown as filled circles in Fig. 1b.

The endocardial model in tissue has a $\mathrm{d}v/\mathrm{d}t_{max}$ of 232 V/s, close to the value of 234 ± 28 V/s measured experimentally by Drouin et al. (1995) and to the measurement of 231 ± 30 V/s from Pereon et al. (2000). Its phase 0 amplitude is 126 mV, which is in good agreement with experimentally observed values of 119 mV (Nabauer et al., 1996) and 123 mV (Li et al., 1998). The plateau voltage occurs at 30 mV, closely matching the value of 36 mV of Nabauer et al. (1996) and the value of 29 mV of Li et al. (1998). At a frequency of 1 Hz, APD_{90} is 260 ms compared to 263 ± 33 ms from Li et al. (1998). The steady-state APD restitution curve was calculated to fit the experimental values from Li et al. (1998), Koller et al. (2005), and Pak et al. (2004), which are shown as empty circles in Fig. 1b.

The midmyocardial model in tissue has a $\mathrm{d}v/\mathrm{d}t_{max}$ of 326 V/s, reproducing the experimental value of 326 ± 16 V/s (Drouin et al., 1995). The amplitude of phase 0 is 132 mV, which closely matches the values of 128 mV shown by Li et al. (1998). For the steady-state APD restitution curve with DIs less than 1 s, we only found values for frequencies of 1 and 2 Hz (Drouin et al., 1995; Li et al., 1998). Many different curves can be created to pass through only two points, so the model was further constrained to produce a curve with shape similar to that observed in canine preparations (Gussak and Antzelevitch, 2003), where at short DIs the APD

Table 2
Summary of model properties

	PB	BWZVP	TNNP			IMW	MV		
			Epi	Endo	M		Epi	Endo	M
Number of model variables	22	6	17	17	17	67	4	4	4
Single cell									
10 s of numerical simulation	6.5 s	1.3 s	4.1 s	4.1 s	4.1 s	1051 s (17.5 min)	0.13 s	0.13 s	0.13 s
10 s of simulation (optimized code)	1.5 s	0.3 s	0.9 s	0.9 s	0.9 s	2.4 s	0.06 s	0.06 s	0.06 s
Resting membrane V (mV)	−90.6	−90.6	−86.3	−86.1	−86.1	−90.6	−83	−83	−83
Phase 0 amplitude (mV)	140.1	138	124.6	124.6	125.5	125.6	126	128	133
Tissue									
Phase 0 amplitude (mV)	113	115	107.6	111.85	106.7	114	122	126	132
$(dv/dt)_{max}$ (V/s)	325	381	261	261	263.8	287	227	232	326
APD_{90} (at 1 s BCL) (ms)	394	418	260	260	307	322	269	260	410
APD_{min} ($S1$–$S2$) (ms)	292	298	221	221	248.5	299	216	186	255
DI_{min} ($S1$–$S2$) (ms)	13	13	39.8	39.8	41.78	54	58	35	36
CV_{max} ($S1$–$S2$) (cm/s)	58	58	58.8	58.8	58.8	57	69.4	70	80
CV_{min} ($S1$–$S2$) (cm/s)	50	50	40	40	41	42	34	32	36
Dominant frequency in 2D (Hz)	3.27	3.49	3.86	3.84	3.36	10.2, 6.5, and 3.5	3.38	3.77	3.0

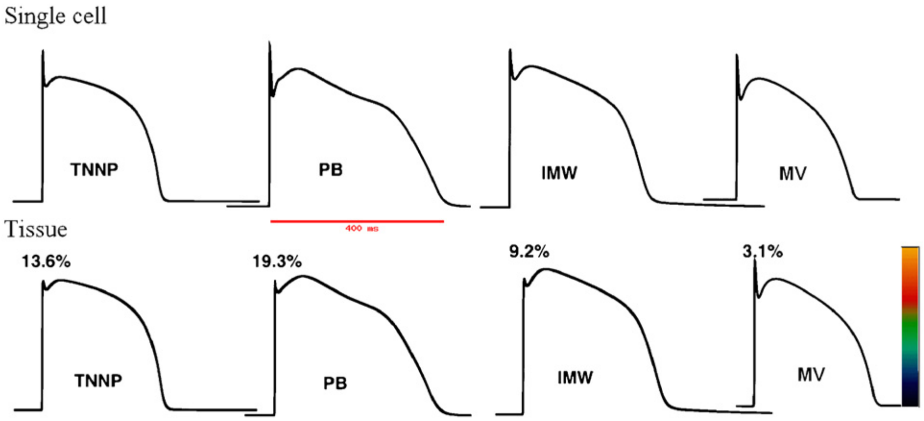

Fig. 2. Action potentials for four human ventricular models in single cells (top) and in tissue (bottom). All action potentials are shown after pacing to steady state at a CL of 1 s. Because of electrotonic coupling effects, all of the model APs lose amplitude in tissue compared to in single cells, with the PB model decreasing the most (19.3%) followed by the TNNP (13.6%), IMW (9.2%), and MV (3.1%). Action potential shapes differ among the models but largely remain the same in tissue apart from the upstroke height, which is lower than the plateau for the TNNP, PB and IMW models. Color bar shows the voltage color scale used in Figs. 5, 6, 8 and 10. Scale bar represents 400 ms.

restitution curve approaches those of the epicardial and endocardial cells, while still passing through the average values of Drouin et al. (1995) and Li et al. (1998) at frequencies of 1 and 2 Hz. It is important to note that in contrast to canine ventricular cells, where midmyocardial cells feature a prominent spike-and-dome morphology (Gussak and Antzelevitch, 2003), human midmyocardial cell APs have not been reported to possess a prominent notch (Drouin et al., 1995, 1998; Li et al., 1998).

For the three cell types, the resting membrane potential was set to −83 mV, which is the average of the resting membrane potential values reported by Drouin et al. (1995), Peeters et al. (1995), Nabauer et al. (1996), Li et al. (1998), and Pereon et al. (2000). In addition, the threshold for excitation in all three cell types was set to −60 mV, which matches the activation of the fast inward Na^+ current in human cardiac cells (Sakakibara et al., 1993).

3.2. Comparison of action potentials

The other three ventricular models exhibit epicardial APs of different morphologies compared to the minimal model and the experimental data on which it is based. Fig. 2 shows APs in single cells and in tissue for the TNNP, PB, IMW, and minimal models at a CL of 1 s. The TNNP model AP has a flatter plateau than the other models, while the PB has a substantially longer duration and a pronounced biphasic repolarization. The IMW AP is also fairly long in comparison with the TNNP and minimal models.

When coupled into tissue, any model experiences a decrease in the amplitude of the AP upstroke because of electrotonic currents that depolarize neighboring excitable cells. An important difference among the models is the percentage of upstroke amplitude that is lost in tissue due to coupling. At a CL of 1 s, the reductions are 13.6, 19.3, 9.2, and 3.1 percent of the phase 0 amplitude of a single cell for the TNNP, PB, IMW, and minimal models, respectively. In the TNNP, PB, and IMW models, the upstroke amplitude decreases so much in tissue that the upstroke peak falls below the maximum voltage of the plateau (Fig. 2), a property that none of the models exhibit in a single cell at this CL. This dramatic decrease in the AP amplitude in tissue does not seem to be consistent with APs recorded in tissue (Peeters et al., 1995; Iost et al., 1998). On the other hand, the minimal model agrees with experiments in that its maximum upstroke voltage remains higher than the plateau voltage in tissue. A comparison of other important characteristics among the models is summarized in Table 2.

Please cite this article as: Bueno-Orovio, A., et al., Minimal model for human ventricular action potentials in tissue. J. Theor. Biol. (2008), doi:10.1016/j.jtbi.2008.03.029

3.3. Restitution of APD and CV

The models all have different adaptations to changes in rate, as illustrated in the restitution curves shown in Fig. 3. In panel A, APD restitution curves are shown for all the epicardial models along with the experimental data points from Morgan et al. (1992) shown with filled circles. Several important differences can be seen among the curves. Both the TNNP and minimal models reproduce the restitution curve with a high degree of accuracy as they were designed to fit this particular data set, with the minimal model passing through more of the data points at long and short CLs. The IMW and PB models, however, produce APs that are much longer than the experimental values. The PB model in particular shows much longer APDs than those observed experimentally, while the IMW restitution curve is relatively flat, even at short DIs. The minimum DI also differs among the models (see Table 2), with the PB model having the smallest DI$_{min}$. The different rate dependence exhibited by the models is associated primarily with the different roles played by the L-type calcium current $I_{\mathrm{Ca,L}}$ and the rapid and slow delayed rectifiers I_{Kr} and I_{Ks}. As shown in Fig. 4, it is primarily peak $\mathrm{I_{Ca,L}}$ (in conjunction with the transient outward current I_{to} that opposes it) that varies with rate for the IMW and TNNP models, which gives rise to relatively flat APD restitution curves because the currents are primarily the same magnitude during the plateau and repolarization; only the different height of the plateau varies, which shifts the onset of repolarization. Only at the most rapid CLs do repolarization currents increase (I_{Kr} for the TNNP model and I_{Ks} for the IMW model) to produce a slightly sloped section of the restitution curve. The TNNP model restitution curve is also flattened by the reduction in repolarizing I_{Ks} at short CLs. In contrast, I_{Kr} and I_{Ks} are strongly rate-dependent over the entire AP for the PB model, which, in combination with differences in $I_{\mathrm{Ca,L}}$, gives rise to a steeper restitution curve.

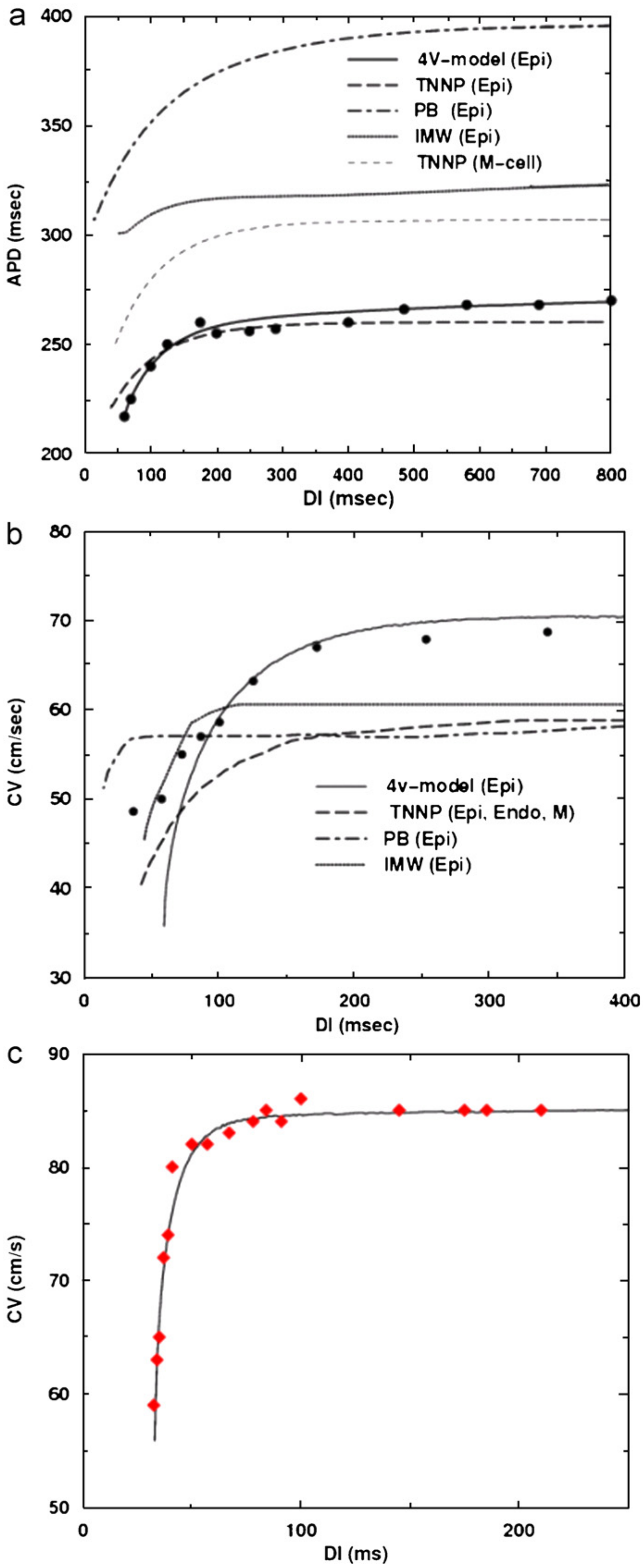

Fig. 3. APD and CV restitution curves for four models of human ventricular myocytes obtained in tissue using an $S1$–$S2$ protocol with $S1 = 1$ s: (a) APD restitution curves are for epicardial cells from the MV, TNNP, PB, and IMW models. Experimental data from human epicardial cells/tissue as used by Ten Tusscher et al. (2004) from Morgan et al. (1992) are shown as solid black circles for comparison. The PB model has extremely long APDs, longer than all the other models. The models also have different values of DI$_{min}$, with the PB model capable of activation at the smallest DIs. (b) CV restitution curves, using a diffusion coefficient of 1.171 cm^2/s. The MV model has the largest CV$_{max}$ value, closest to that of the experimental data used in Ten Tusscher et al. (2004), which used a rescaled guinea pig ventricular tissue (Girouard et al., 1996) that matches reported human ventricular CV$_{max}$ of about 70 cm/s (Taggart et al., 2000) (shown as solid black circles). The MV and TNNP CVs by construction varied the most over a wider range of DIs. The PB model's CV restitution is nearly flat except for the last 20 ms, and the IMW model's varies little and shows a slight supernormality at DIs around 190 ms before a fast decrease of about 10 cm/s over a DI range of about 20 ms. (c) CV restitution curve for the minimal model using the epicardial parameter set with $\tau_{v1}^{-} = 10$ and $\tau_{v2}^{-} = 20$ to match one of the CV restitution curves obtained by Yue et al. (2005) in the left ventricle. Here the diffusion coefficient $D = 1.68$ cm^2/s was used to match the maximum CV of 85 cm/s.

For the MV model, the slopes of the restitution curves for epicardial and endocardial data are greater than one, with maximum slopes of 3.5 and 6, respectively. However, the slope is greater than one only over a very narrow range of DIs, between 58 and 63 ms for the epicardial model and between 35 and 46 ms for the endocardial model. The midmyocardial MV model has slope less than one for all DIs.

CV restitution in human ventricles has not yet been well characterized. The CV of paced wavefronts has been observed to vary from a large maximum CV of 70 cm/s (Taggart et al., 2000) or 87 cm/s (Nanthakumar et al., 2007) to a minimum of 41 cm/s (Nanthakumar et al., 2007). Using the diffusion coefficient calculated in Appendix A specifically for human ventricular tissue, ($D = 1.171 \pm 0.221$ cm^2/s) the maximum and minimum CVs, respectively, for the models are 70 and 34 cm/s (MV), 57 and 42 cm/s (IMW), 59 and 40 cm/s (TNNP) and 58 and 50 cm/s (PB). The minimal model has the largest CV$_{max}$ of all the models as well

Please cite this article as: Bueno-Orovio, A., et al., Minimal model for human ventricular action potentials in tissue. J. Theor. Biol. (2008), doi:10.1016/j.jtbi.2008.03.029

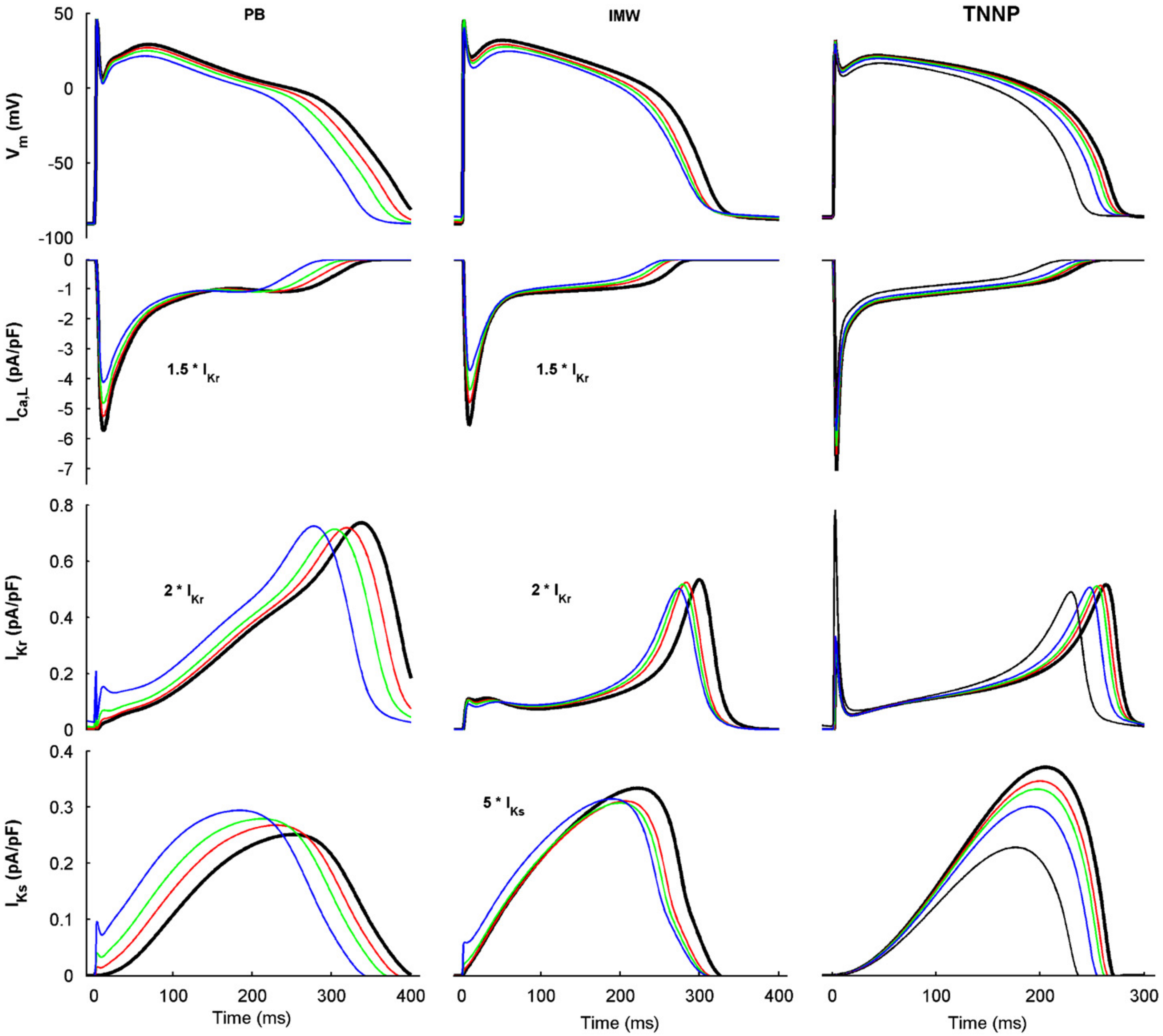

Fig. 4. Rate dependence of action potentials and key transmembrane currents for the PB, IMW, and TNNP models for cycle lengths of 1000 ms (black), 600 ms (red), 500 ms (green), 400 ms (blue), and 300 ms (purple, TNNP only). While $I_{\mathrm{Ca,L}}$ is involved in all cases in setting the height of the plateau, I_{Kr} and I_{Ks} only show rate dependence over the full range of CLs for the PB model, which explains its greater rate dependence (see Fig. 3a). Note that the shorter action potential and associated currents for the TNNP model are shown over 300 ms, while the time duration for the PB and IMW models is 400 ms. Several currents are magnified by showing them multiplied by a constant factor, as indicated, to allow rate differences to be seen.

as a larger range of CV values, comparable to the experiments of Nanthakumar et al. (2007).

As in Ten Tusscher et al. (2004), in the absence of detailed and reliable human ventricular CV restitution data, a rescaled experimental guinea pig CV restitution curve (Girouard et al., 1996) with a maximum CV of 70 cm/s (Taggart et al., 2000) is used as a first approximation of CV data to be compared with the models. Fig. 3b shows how the CV varies significantly in experiments over a broad range of DIs, a property reproduced by both the minimal and TNNP models. In contrast, the IMW model and, especially, the PB model have very flat CV restitution curves, with only a small difference in CV occurring at the smallest DIs.

While Nanthakumar et al. (2007) report a gradual change in CV restitution using optical mapping, Yue et al. (2005) using non-contact mapping found CV restitution curves to be mostly constant with changes over only a small region of DIs. These restitution curves, however, were measured using an $S1$–$S2$ protocol, not a steady-state protocol, and for only one value of $S1$. As will be discussed below in Section 3.6, memory effects can potentially alter $S1$–$S2$ restitution curves depending on the value of $S1$. Nonetheless, the minimal model was fitted to reproduce one of the CV restitution curves of Yue et al. (2005) obtained in the left ventricle, as shown in Fig. 3c. This curve is obtained using the epicardial parameter values (Table 1) with $\tau_{v1}^{-} = 10$ and $\tau_{v2}^{-} = 20$.

3.4. *Reentry dynamics*

The dynamics and stability of reentrant spiral waves in two dimensions also differ among the models. Fig. 5 shows

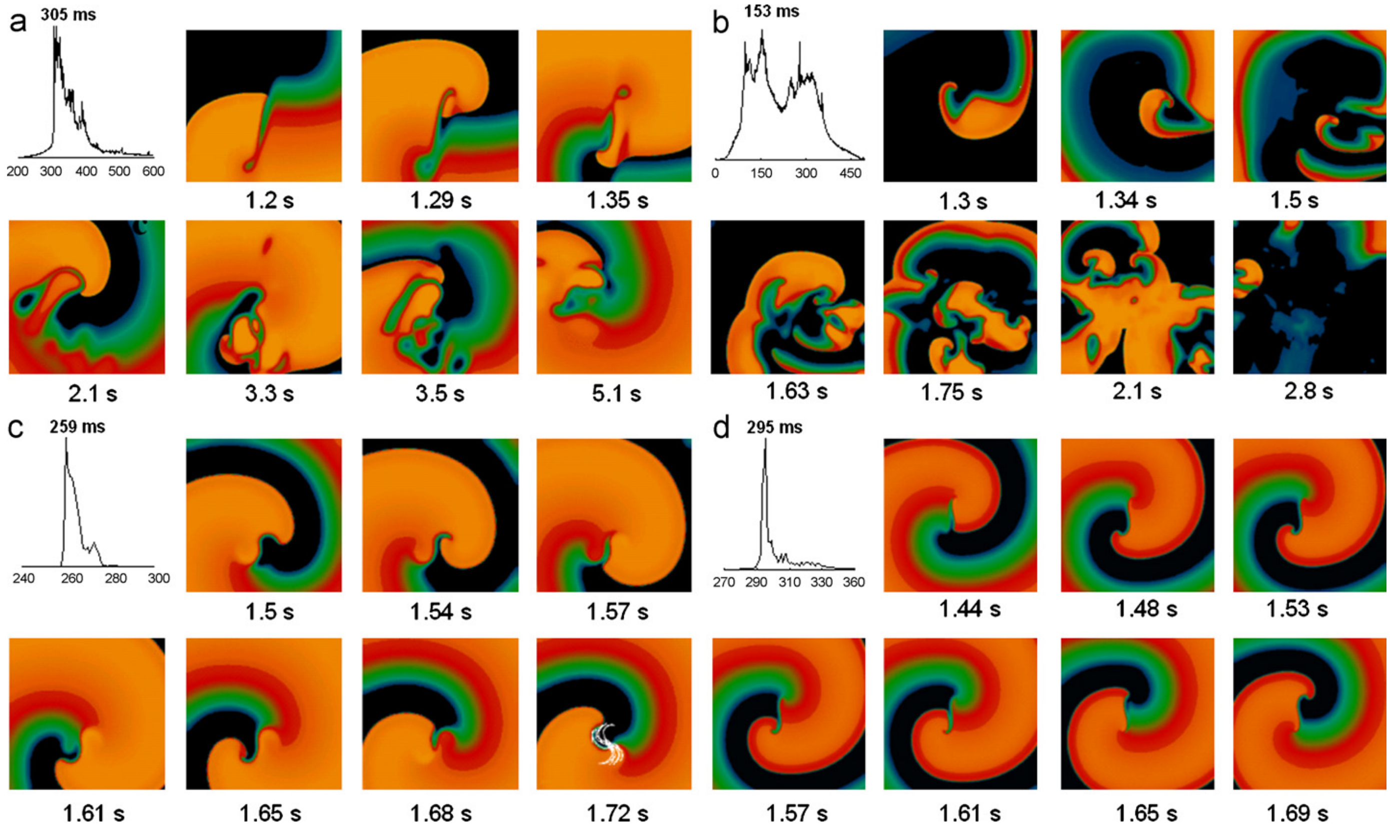

Fig. 5. Reentrant spiral wave dynamics in 2D for four models of human ventricular myocytes: (a) The PB model exhibits quasi-breakup with wave fronts that often stall and reform. The dominant period over 10 s of simulation is 305 ms. (b) The IMW model develops sustained breakup, with narrow wavelengths that give three major dominant periods, the largest at about 98 ms and the other two at 153 and 285 ms. (c) The TNNP model remains stable with a slowly precessing linear core and a dominant cycle length of 259 ms. (d) The minimal model is also stable with a linear core, and dominant cycle length slightly higher than the TNNP of 295 ms. Epicardial parameter sets were used for the TNNP and the minimal model. Tissue sizes were 800 × 800, 700 × 700, 600 × 600, and 500 × 500 for the PB, IMW, TNNP, and MV models, respectively.

representative spiral wave dynamics for the four models. The PB model exhibits quasi-breakup, with wave fronts that often encounter refractory tissue, separate, and then re-form farther from the original core, as shown in Fig. 5a. However, the excitability of the model and large wavelengths allow them to heal quickly, and during a relatively stable window when there is little breakup a linear core can be estimated of about 6.5 cm (Cherry and Fenton, 2007). While the PB model produces quasi-breakup, the dynamics of the BWZVP model depends on the spatial and temporal resolutions used. At a spatial resolution of 0.025 cm, the model produces stable reentry with a core of about 5.5 cm (Bernus et al., 2002a) and a dominant frequency of 3.39 Hz. However, at a higher spatial resolution of 0.02 cm, an initiated spiral wave loses stability and becomes quasi-stable, as shown in Fig. 6, with a higher dominant frequency (3.49 Hz) and behavior quite similar to that of the original PB model.

The IMW model shows different behavior (Fig. 5b), as the spiral immediately transitions to continuous breakup after initiation, with many extremely small wavelengths and eventual termination of the arrhythmia after a few seconds. The TNNP model remains stable after initialization with a slightly meandering core. After about 20 s, the core trajectory becomes a stable, slowly precessing linear core with a cross section of about 3 cm (Fig. 5c). The minimal model produces dynamics similar to that of the TNNP model, with a stable reentrant wave tracing out a slowly precessing linear core with a cross section of about 3 cm (Fig. 5d). The MV model produces stable reentries for the endocardial and midmyocardial cell types as well. The dominant frequencies of the reentries also vary among the models, as indicated in Figs. 5 and 6 and Table 2.

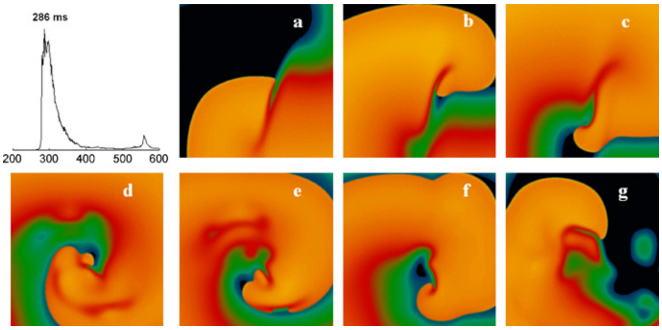

Fig. 6. Reentrant spiral wave dynamics of the reduced PB (BWZVP) model in 2D. Quasi-stable dynamics similar to that of the PB model are obtained, with a dominant period of 286 ms that is slightly shorter than that of the PB model (305 ms). Tissue size is 800 × 800.

While the minimal model produces a stable reentry using a broad CV restitution curve (Fig. 3b), it becomes quasi-stable when fitted to the steeper CV restitution curve of Yue et al. (2005) (Fig. 3c). For the latter case, as shown in Fig. 7, the dynamics is similar to that of the PB model, where quasi-breakup is produced by the longer wavelength (due to the larger CV_{max}) and the decreased DI_{min}, as described previously by Fenton et al. (2002a).

3.5. Transmural heterogeneity and pseudo-ECG

Both the minimal model and the TNNP model include parameter variations to reproduce endocardial and midmyocardial

Please cite this article as: Bueno-Orovio, A., et al., Minimal model for human ventricular action potentials in tissue. J. Theor. Biol. (2008), doi:10.1016/j.jtbi.2008.03.029

cells as well as epicardial. Fig. 8a shows the APD restitution curves of the three cell types for both models, along with experimental data. The minimal model, in contrast to the TNNP model, includes noticeable differences between endocardial and epicardial restitution curves and significantly longer APDs for the midmyocardial cells. In addition, in the minimal model the APDs for endocardial cells are smaller than those for epicardial, matching experimental data (Drouin et al., 1995, 1998; Li et al., 1998; Pereon et al., 2000), while the opposite is true for the TNNP model. The values of dv/dt_{max} for the three cell types in the TNNP model are nearly identical (see Table 2). In contrast, the minimal model produces AP rates of rise (see Table 2) that closely match the experimentally obtained values of 228±11, 234±28, and 326±16 V/s for epicardial, endocardial, and midmyocardial cells, respectively (Drouin et al., 1995).

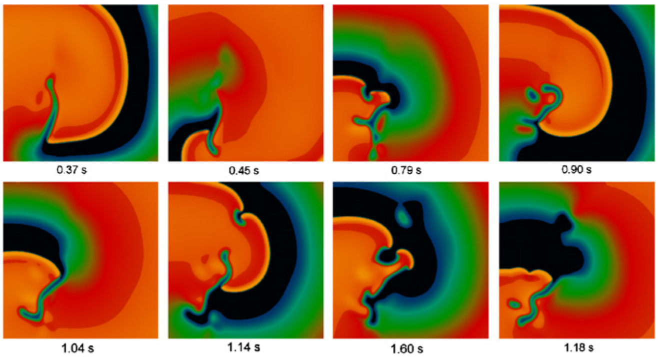

Fig. 7. Reentrant spiral wave dynamics of the minimal model using epicardial parameter values together with the CV restitution curve shown in Fig. 3c. Quasi-stable dynamics similar to that of the PB model are obtained. Tissue size is 600 × 600.

These different cell types were incorporated into a left ventricular wedge preparation for computation of a pseudo-ECG when a wave propagates from endocardium to epicardium. A portion of the LV wall was excised from the porcine ventricular structure of Stevens et al. (2003), and the cell types were assigned within the tissue as described in the Methods according to Drouin et al. (1995) for both the TNNP and minimal models, as shown in Fig. 8b. When the pseudo-ECGs were computed by pacing at a constant CL of 1 s, the minimal model (Fig. 8c) produced a T-wave with a larger magnitude than that produced by the TNNP model (Fig. 8d). The longer APDs of midmyocardial cells in the minimal model resulted in the increased T-wave magnitude.

3.6. Memory

The TNNP and IMW models exhibit a substantial degree of short-term cardiac memory. These effects can be seen by plotting $S1$–$S2$ restitution curves calculated in a 1D cable as described in the Methods for different values of the $S1$ CL. Fig. 9a shows

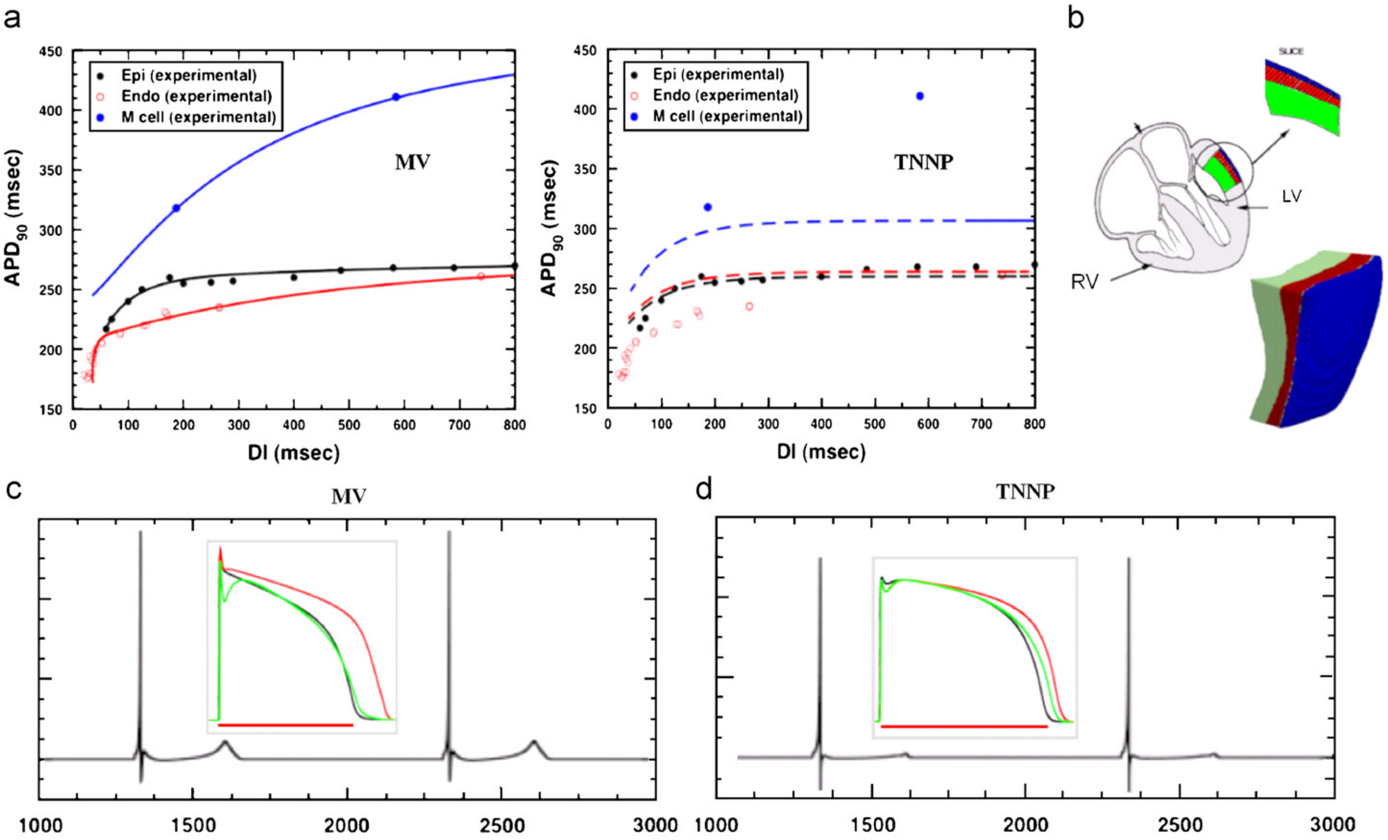

Fig. 8. Epicardial, endocardial, and midmyocardial cells for the TNNP and MV models: (a) APD restitution curves for the minimal model (left) and for the TNNP model (right). Data for epicardial (black), endocardial (red), and midmyocardial (blue) cells are shown in both cases. Experimental restitution data as in Fig. 2 are shown as filled circles for reference in both panels. The MV model shows a much greater difference between midmyocardial cells and the other cell types than the TNNP model and also has distinct curves for epicardial and endocardial cells. (b) Representation of the distribution of epicardial (blue), midmyocardial (red), and endocardial (green) cells (Drouin et al., 1995) within a 3D slab of tissue from a porcine left ventricle (Stevens et al., 2003) used to simulate pseudo-ECGs. (c) Pseudo-ECG obtained in the geometry shown in B using the MV model with endocardial (black), epicardial (green), and midmyocardial (red) cells with action potentials recorded in tissue as shown in the inset (time scale bar represents 270 ms). (d) Pseudo-ECG obtained using the TNNP model with endocardial (black), epicardial (green), and midmyocardial (red) cells with action potentials recorded in tissue as shown in the inset (time scale bar represents 270 ms). In both cases, the pseudo-ECG was calculated during two successive stimuli that originate at the center of the endocardial surface at a cycle length of 1 s.

Please cite this article as: Bueno-Orovio, A., et al., Minimal model for human ventricular action potentials in tissue. J. Theor. Biol. (2008), doi:10.1016/j.jtbi.2008.03.029

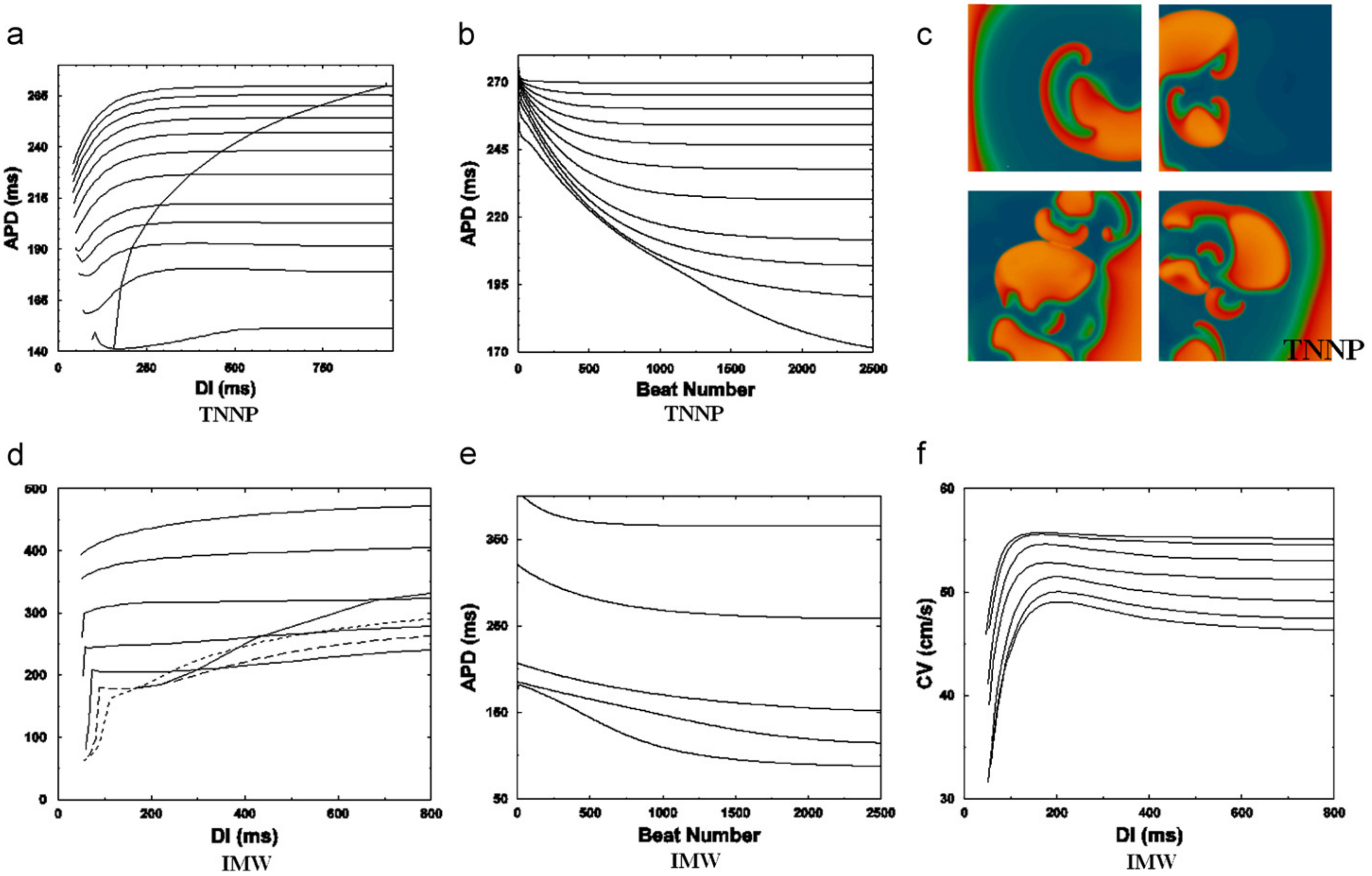

Fig. 9. Memory effects in the TNNP and IMW models in tissue: (a) $S1$–$S2$ restitution curves for the TNNP model obtained at different $S1$ cycle lengths and the steady-state restitution curve shown as a thicker line. $S1$–$S2$ curves, from top to bottom, are for $S1$ cycle lengths of 1.2, 1.1, 1, 0.9, 0.8, 0.7, 0.6, 0.5, 0.45, 0.4, 0.35, and 0.3 s. (b) APD adaptation to cycle length of the TNNP model from the initial conditions reported by Ten Tusscher et al. (2004) after pacing for 2500 beats at CLs of 1.2, 1.1, 1, 0.9, 0.8, 0.7, 0.6, 0.5, 0.45, 0.4, and 0.35 s. (c) Four frames showing the dynamics of a spiral wave in the TNNP model after initiation in the same manner as in Fig. 5c but after pacing at a CL of 300 ms for 2500 beats. (d) $S1$–$S2$ restitution curves obtained for the IMW model at different $S1$ cycle lengths and the steady-state restitution curve shown as a thicker line. $S1$–$S2$ curves with $S1$ CLs of 4, 2, 1, 0.667, and 0.5 s (solid) decrease with $S1$ CL, while curves with $S1$ CLs of 0.4 s (long dashes) and 0.333 s (short dashes) show APDs that increase with $S1$ CL. APDs decrease with $S1$ cycle lengths except at short $S1$'s where they start to grow for large DI's. (e) APD adaptation to cycle length of the IMW model from the original initial conditions reported by Iyer et al. (2004) after pacing for 2500 beats. CLs are 2, 1, 0.5, 0.4, and 0.333 s. (f) $S1$–$S2$ CV restitution curves for the IMW model for $S1$ CLs of 4, 2, 1, 0.667, 0.5, 0.4, and 0.333 s, from top to bottom.

a family of $S1$–$S2$ restitution curves for the TNNP model in tissue, ranging from a maximum $S1$ CL of 1.2 s (top) to a minimum of 0.3 s (bottom). The solid curve shows the steady-state APD restitution curve. Fig. 9b shows the time of accommodation to a new CL as a function of beat number for each of the CLs of Fig. 9a starting from the steady state obtained after pacing at a CL of 1.2 s. The APDs at all DIs decrease as the $S1$ CL is decreased, but the shapes of the curves vary from monotonically decreasing to biphasic. The APD obtained in an $S1$–$S2$ restitution curve depends quite strongly on the $S1$ value and the "memory amplitude" (defined in Cherry and Fenton, 2007) is about 120 ms, with APDs ranging from 270 to 150 ms at long DIs.

The IMW model also exhibits strong memory effects, with nearly flat $S1$–$S2$ restitution curves that decrease in APD by more than 200 ms for long DIs as the $S1$ CL is decreased from 4 s to 333 ms, as shown in Fig. 9d. Note that as CL decreases, so do the APD restitution curves, until a CL of 500 ms. For $S1$–$S2$ restitution curves obtained using CLs of 400 and 333 ms, the curves go up, corresponding to increased APDs, as has been observed previously in other models (Cherry and Fenton, 2007). Fig. 9e shows the time of accommodation as a function of beat number for five of the CLs of Fig. 9d starting from their respective single-cell initial conditions given in the original paper (Iyer et al., 2004) and the authors' website.

Memory also can affect the dynamics of reentrant waves through the initial conditions used during initiation. The TNNP model, for example, produces a stable spiral wave when initiated using initial conditions corresponding to steady state at a CL of 1000 ms. However, if the tissue is first paced for 2500 beats to a steady state at a CL of 300 ms, an initiated spiral wave quickly breaks up, as shown in Fig. 9c, with complex dynamics that last for several seconds within the domain before self-terminating.

The TNNP and IMW models also exhibit a novel phenomenon of memory in CV restitution. Fig. 9f shows different CV restitution curves obtained using $S1$–$S2$ protocols for the IMW model for the seven $S1$ CLs shown in Fig. 9d. As the $S1$ CL decreases, so does the CV, by as much as 9 cm/s, or about 17%, at long DIs. This type of memory has been postulated before (Fenton et al., 1999) but has not been observed previously for any model or experimentally. The TNNP model also exhibits memory in CV restitution (not shown), but to a smaller degree. The CV restitution curves remain almost constant for S1 CLs above 700 ms, and for shorter CLs the CVs decrease in a manner similar to that shown by the IMW model from a maximum CV of 55.4 to 47.5 cm/s (a decrease of 7.9 cm/s, or about 14%) and from a minimum CV of 38.5 to 31.2 cm/s (a decrease of 7.3 cm/s). Memory in CV restitution arises in these models primarily due to the intracellular sodium concentration Na_i, which increases as the CL is decreased. For

Please cite this article as: Bueno-Orovio, A., et al., Minimal model for human ventricular action potentials in tissue. J. Theor. Biol. (2008), doi:10.1016/j.jtbi.2008.03.029

example, in the IMW model the maximum CV obtained in *S*1–*S*2 restitution curves (obtained at long DIs) is not constant, as shown in Fig. 10a. It decreases 16 percent when the *S*1 CL is decreased from 4000 to 333 ms. However, the change in CV is only 4 percent as the *S*1 CL is decreased over the same range when Na_i is held fixed at its diastolic value from steady state pacing at a CL of 4000 ms. Similar variations in the range of CV values are seen when Na_i is fixed to other values, including the diastolic values for CLs of 1000 and 500 ms. In the same way, holding Na_i fixed to the diastolic value obtained at 1000, 500, or 350 ms in the TNNP model results in a 1 percent change in maximum CV over S1 CLs between 1000 and 350 ms, compared to a 6 percent decrease under normal conditions, as shown in Fig. 10b.

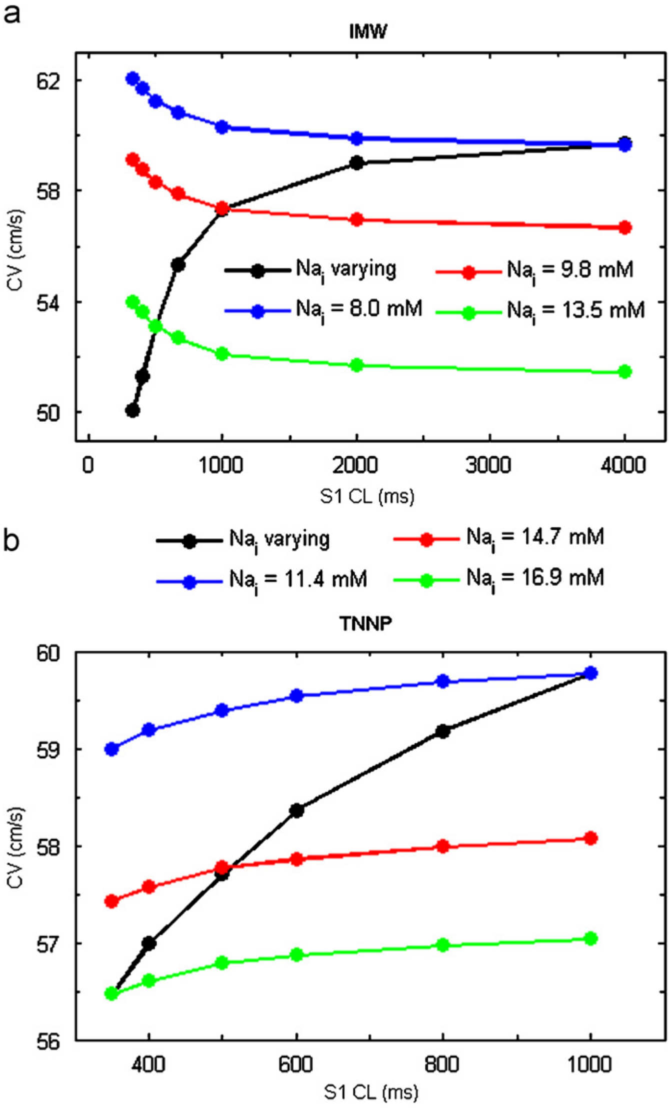

Fig. 10. Dependence of CV restitution in the TNNP and IMW models on intracellular sodium: (a) Fixing Na_i to the diastolic values obtained from steady-state pacing at CLs of 4000 ms (blue), 1000 ms (red), and 500 ms (green) decreases the variability in CV_{max} obtained over a range of *S*1 CLs in the IMW model compared to the normal case (black), in which Na_i accumulates at short CLs and leads to reduced CV_{max}. The increase, rather than decrease, in CV_{max} as the *S*1 CL is decreased with Na_i fixed is associated with the supernormal regions in CV restitution for this model, as shown in Fig. 8f. (b) Holding Na_i fixed to the diastolic values obtained from steady-state pacing at CLs of 1000 ms (blue), 500 ms (red), and 350 ms (green) decreases the variability in CV_{max} obtained over a range of *S*1 CLs in the TNNP model compared to the normal case (black), in which Na_i accumulates at short CLs and leads to reduced CV_{max}. For both models, the DI was held fixed to 850 ms in all cases, which produces a maximal value of CV for each *S*1 CL.

3.7. *Parameter fittings to other models*

Just as the minimal model parameters were fitted to experimental data, parameter values can be calculated to fit the restitution curves of other models and to reproduce their spiral wave dynamics. Fig. 11 shows spiral wave dynamics for the TNNP and PB models along with similar dynamics for the minimal model using the fitted parameters for these two models (Table 2). In Fig. 11a, the stable spiral wave of the TNNP model is reproduced by the minimal model fit. Similarly, the quasi-stability of the PB model, with stalling and recombining fronts, is reproduced by the minimal model when fitted to the PB model (Table 2), as shown in Fig. 11b.

4. Discussion

4.1. *Model structure*

We have presented a minimal ventricular model, in the sense that it contains the minimum number of differential equations necessary to accurately reproduce experimentally measured properties for human epicardial, endocardial, and midmyocardial cells in tissue (Fig. 1). The model is intended primarily to reproduce realistic tissue-level properties of cardiac APs and considers not all the individual cell currents, but a total transmembrane current summed in three categories, fast inward, slow inward, and outward. Therefore, just like other ionic models are designed to reproduce overall cellular currents and membrane potential without including thousands of individual ion channels (e.g., about 5 Ca^{2+} channels/$\mu\mathrm{m}^2$ and 16 Na^+ channels/$\mu\mathrm{m}^2$ (Reuter, 1984)) and cannot be used to study or simulate intracellular dynamics like intracellular calcium waves or variations in membrane potential across a single cell, the minimal model is limited in that changes to the dynamics of a particular ion channel, such as blockage of a channel, cannot be incorporated by changing or blocking a given conductance. Nevertheless, the minimal model can be fitted to data recorded under the conditions of interest, such as after administration of a pharmacological agent (Fenton et al., 2002b) or within tissue that has genetic mutations like the Brugada syndrome (Fenton et al., 2004). Moreover, the minimal model has the advantages of being more computationally tractable to allow for large-scale tissue simulations as well as having improved flexibility to model variations in electrophysiological properties, as shown in Fig. 1, where the model reproduces not only the AP morphologies of epicardial, endocardial, and midmyocardial cells, but also APD restitution curves selected from the literature. In addition, this flexibility permits modeling of any experimentally measured gradients in properties, such as spatial dependence of APD restitution properties (Nash et al., 2006) as well as apico-basal and transmural gradients, with greater ease.

Compared to other ionic models of human ventricular APs, the minimal model, by construction, achieves more accurate quantitative agreement with experimental tissue properties. For example, in contrast to the TNNP epicardial, endocardial, and midmyocardial cell formulations, which all have almost the same amplitude and dv/dt_{max}, the minimal model has different amplitudes and maximum upstroke velocities that match experimentally observed characteristics. They also show a larger variation in APD, which may be necessary to reproduce accurate dispersions within the ventricles and to calculate realistic ECGs

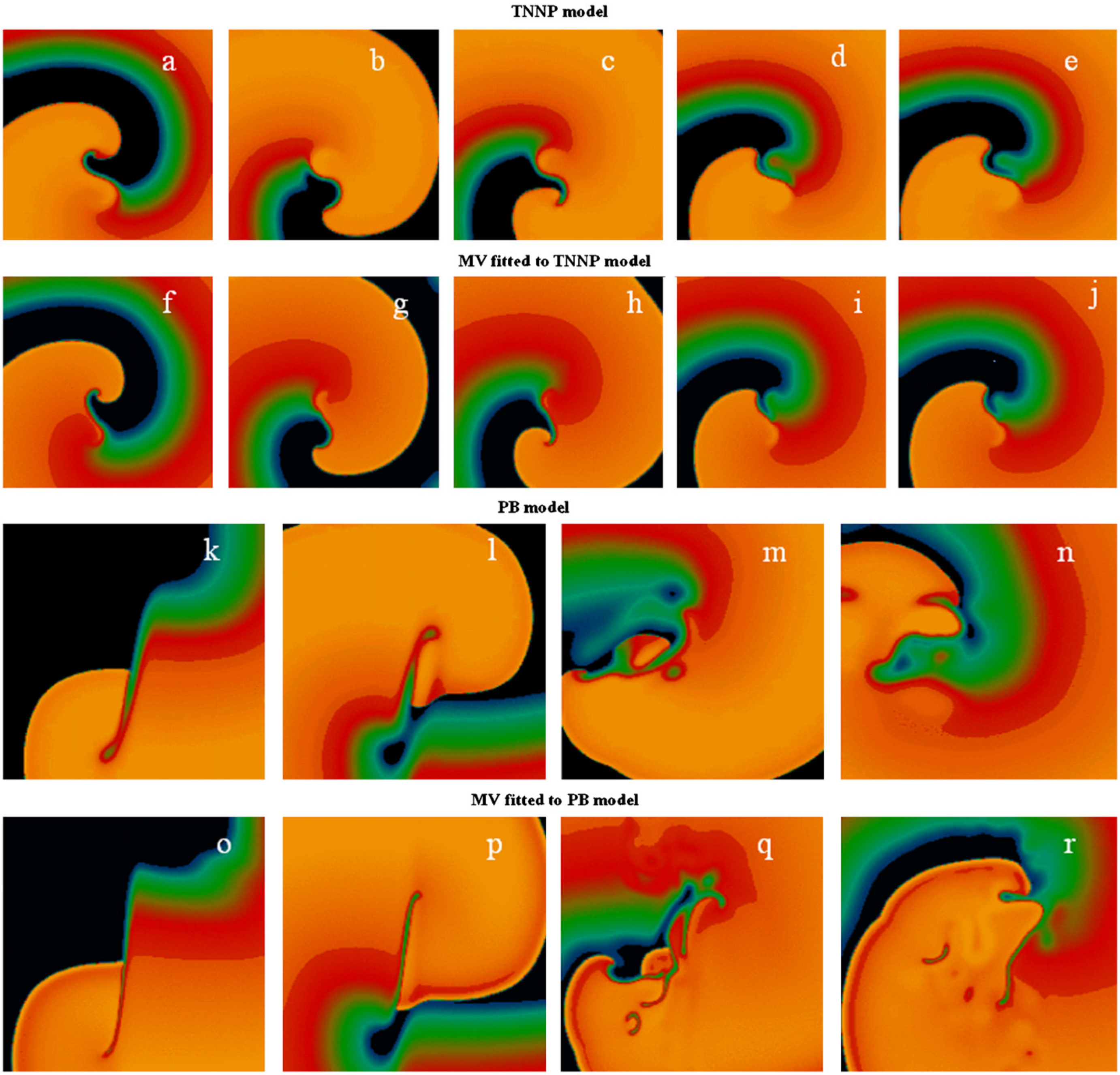

Fig. 11. MV model fitted to reproduce the dynamics of the TNNP and PB models. Reentrant waves in the original TNNP model (a–e) and MV-TNNP model (f–j) show similar stable spiral wave dynamics. Reentrant waves in the original PB model (k–n) and MV-PB model (o–r) show similar quasi-breakup dynamics, with a long linear core combined with a small DI that allows frequent wave front–back interactions. While many of the wave breaks heal quickly, the spiral waves are never completely stable. Tissue sizes were 600 × 600 for the TNNP and MV-TNNP models and 800 × 800 for the PB and MV-PB models.

(Gima and Rudy, 2002; Gussak and Antzelevitch, 2003), as shown in Fig. 8. The different AP morphologies of the cell types are closer to experiments for the minimal model than for the TNNP model, as shown in Figs. 1 and 8. In addition, human midmyocardial cells (Drouin et al., 1995, 1998; Li et al., 1998) and the minimal model, unlike canine midmyocardial cells (Gussak and Antzelevitch, 2003) and the TNNP model, do not show a pronounced AP notch. In the TNNP model the epicardial APD is smaller than the endocardial; however, in the MV model it is the opposite, consistent with what has been observed experimentally (Drouin et al., 1995, 1998; Li et al., 1998; Pereon et al., 2000).

For the TNNP, IMW, and PB epicardial cell models, the value of dv/dt_{max} (see Table 2) in tissue is higher than for the minimal model and in experiments (Drouin et al., 1995; Pereon et al., 2000), but for each the maximum voltage during the upstroke occurs below the plateau voltage (Fig. 2), which differs from some experimental observations (Peeters et al., 1995; Iost et al., 1998). The APD restitution curves are different for the models, which can be expected as different models may be based on data from different experiments. However, the PB model values seem to be larger than average, and the IMW model seems to have relatively flat restitution curves as a function of DI (see Fig. 3a).

Please cite this article as: Bueno-Orovio, A., et al., Minimal model for human ventricular action potentials in tissue. J. Theor. Biol. (2008), doi:10.1016/j.jtbi.2008.03.029

Available CV restitution information for human ventricular myocardium is limited. Saumarez et al. (1992, 1995) characterized electrogram latency as a function of $S1$–$S2$ coupling intervals in the RVs of human patients, with latency increasing in normal patients at coupling intervals of 265–284 ms, but their conduction latency data only indirectly indicate CV restitution, and their use of the $S1$–$S2$ coupling interval with no associated APD information prevents DI information from being known. Yue et al. (2005) used noncontact mapping to assess CV restitution curves at 32 different sites in the left and right ventricles. They found that the range of CV values was 25 ± 10 percent of the maximum CV and that steep restitution occurred only for the smallest 10 ± 6 and 38 ± 13 ms ranges of DIs in the left and right ventricles, respectively. Nonetheless, their data also showed substantial variation with recording location, with maximum CV varying between 15 and 90 cm/s. In addition, they used the $S1$–$S2$ protocol with a single value of the $S1$ CL to obtain CV restitution data, which may differ from restitution curves measured using other $S1$ CL values and the steady-state protocol. Other experiments have determined human ventricular CV values including a maximum of 70 cm/s (Taggart et al., 2000) or 87 cm/s (Nanthakumar et al., 2007) and a minimum of 41 cm/s (Nanthakumar et al., 2007), giving a dispersion of between 29 and 46 cm/s (or 41 and 53 percent of the maximum CV). In comparison, the PB, TNNP, and IMW models have dispersions of 8, 19, and 15 cm/s (14, 32, and 26 percent), respectively, while the MV model, with its dispersion of 36 cm/s (49 percent) (Table 2), more closely matches the experimental data of Nanthakumar et al.

4.2. Reentry dynamics and stability

For the first time, the stability of reentrant spiral waves in 2D for the PB and IMW models, and for the TNNP model as a function of initial conditions, has been analyzed and compared, as shown in Fig. 5. It is significant that these three models of human ventricular epicardial cells exhibit three distinct types of reentry behavior in tissue: the PB shows quasi-stability with frequent wavefront stalling and recombining, the IMW model produces sustained breakup, and the TNNP model produces stable or breakup behavior depending on initial conditions. It is possible that the models reflect properties associated with different regions of the epicardium, such as apico-basal, left–right, or anterior–posterior differences. It is also possible that the models were designed primarily for use as isolated myocytes or for slow pacing rates, and it may not be appropriate to extrapolate predictions to rapidly paced tissue.

The PB, TNNP (when stable), and MV models all have well-defined dominant periods, as shown in Fig. 5 (305, 259, and 295 ms, respectively), and all lie well within the tachycardia periods observed clinically, in the range of 240–350 ms (Koller et al., 2005). The BWZVP model dominant period is also in this range both at fine spatial resolutions where breakup occurs (286 ms) and at coarser resolutions where the reentry is stable (303 ms). The IMW model, in contrast (Fig. 5b), has a very broad dispersion of dynamical periods (variability of intervals between excitations), from 40 to 480 ms (with 90% of the periods between 80 and 370 ms), with the maximum and minimum periods beyond the clinical range for both ventricular tachycardia (VT) (maximum period of 350 ms (Koller et al., 2005)) and ventricular fibrillation (VF) (minimum period of 147 ms (Nanthakumar et al., 2007)). Therefore, even considering only the periods that encompass 90% of the full range, the periods displayed by the IMW model vary beyond the values observed for VT and VF at the same time.

The stability of spiral waves in the models is not strictly determined by restitution curve slopes. The MV model has slope greater than one for the epicardial and endocardial cell types, but spiral waves are stable because the spiral wave periods are larger than those of the small region where the slope is steep. Conversely, the PB model, despite having quasi-breakup dynamics, does not have slope greater than one; instead, the small DI_{min} of the PB model, combined with its limited CV restitution, supports frequent wave breaks (Fenton et al., 2002a). Restitution curves for the IMW model are generally flat except for $S1$–$S2$ protocols with short $S1$ CLs at the shortest DIs, just before conduction block. The TNNP model shows the opposite behavior, with slope less than one for $S1$–$S2$ restitution curves, but a steeper slope greater than one for the steady-state curve at DIs below 180 ms. Although steep restitution slopes can be correlated with spiral breakup in some cases, spiral waves may be stable despite steep slopes (Fenton et al., 2002a; Cherry and Fenton, 2004) or may break despite flat restitution (Fenton et al., 1999, 2002a).

4.3. Human ventricular wavelength

Although it has not been discussed previously, it is clear that *in silico* modeling and simulation used to describe arrhythmia mechanisms to date have used models with APDs that are relatively small compared to human ventricular APs (especially at short DIs) and with CV restitution curves with comparatively low maximum longitudinal CV values on the order of 40–50 cm/s. Normal human ventricular APDs are fairly long, around 200 ms in duration even at short DIs, and the CV is quite high. This means that human ventricular wavelengths are much larger than what has been simulated, and it is possible that different mechanisms than what have been studied may give rise to arrhythmias at the longer wavelengths characteristic of human ventricular tissue. Consequently, it may be the case that in normal human ventricles, breakup is more similar to what is observed for the PB model and for the minimal model fitted to the steeper CV restitution curve of Fig. 3b, where long wavelengths and very small values of DI_{min} facilitate interactions between the wave front and back and produce localized conduction blocks (Fenton et al., 2002a). This effect may be amplified by any dispersion of APD, as observed experimentally (Nash et al., 2006) and in simulations (Fenton et al., 2002a, b), even without the need for steep APD restitution curves (Nash et al., 2006). The long human ventricular wavelength has important implications for studies of fibrillation mechanisms.

4.4. Memory

Although it has been shown that the IMW model possesses memory (Iyer et al., 2004), we show for the first time that the TNNP model also possesses a large degree of memory as well (see Fig. 9a). For the TNNP model, the $S1$–$S2$ APD restitution curves decrease with decreasing $S1$ CL; however, for the IMW model this only happens for CLs up to 500 ms. At lower CLs, the $S1$–$S2$ curves reverse and start to go up. Even though this effect has been observed in other ionic models (Cherry and Fenton, 2007), it is still not known if this effect occurs experimentally.

While it is important for models to incorporate short-term memory effects, much more study is needed to understand the mechanisms responsible for memory and the full range of effects memory can produce. Until a detailed quantification of short-term memory is obtained experimentally, validation of model memory properties cannot be performed.

We also show for the first time the phenomenon of memory in CV restitution curves. Just as for APD restitution curves, $S1$–$S2$ CV restitution curves can show different values of CV for the same values of DI and thus indicate that CV, like APD, is dependent on pacing history. Both the TNNP and IMW models exhibit

Please cite this article as: Bueno-Orovio, A., et al., Minimal model for human ventricular action potentials in tissue. J. Theor. Biol. (2008), doi:10.1016/j.jtbi.2008.03.029

a dependence of CV restitution on the $S1$ CL, with the IMW producing the larger difference between CV curves, as shown in Fig. 9f. This memory arises from the increase in intracellular Na^+ that occurs during rapid pacing and could play an important role not only during reentry initiation, when different CLs and DIs may be sampled in rapid succession, but also during alternans development, where it has been shown that CV restitution can play an important role (Watanabe et al., 2001; Qu et al., 2000; Fenton et al., 2002a; Cherry and Fenton, 2004).

4.5. *Importance of initial conditions*

The TNNP model shows the effects that memory, in the form of initial conditions, can have on reentry dynamics. Initiating a spiral wave using initial conditions corresponding to steady state at a CL of 1000 ms results in a stable spiral wave that over 20 s develops a precessing linear core. If instead initial conditions obtained after pacing at a CL of 300 ms for 2500 beats in tissue are used, spiral wave breakup occurs. Because the breakup that occurred self-terminated spontaneously in all cases tested, it is not known yet whether a larger tissue size will allow breakup to be sustained indefinitely, or whether the spiral wave dynamics will transition after some time to a single stable spiral.

4.6. *Model complexity and computational efficiency*

As mentioned by Ten Tusscher et al. (2006), an important difference between models is their complexity and their suitability for performing large-scale simulations. The computational demands of the human ventricular models discussed cover a wide range, as shown in Table 2. Without optimizations, 10 s of simulation in a single cell can require anywhere from 0.13 s (minimal model) to as long as 17.5 min (IMW model), or 8000 times longer. Using the code optimizations described in Section 2.3, all the models can be integrated with a time step of 0.01 ms, and the time required to simulate 10 s decreases substantially, to as little as 0.06 s for the minimal model, with the BWZVP, TNNP, PB, and IMW models requiring 5, 15, 25, and 40 times longer, respectively. For example, a simulation of 600 ms in an anatomically realistic 3D model of human ventricles composed of 12 million nodes would require approximately 20 days using the IMW model or 7 days using the TNNP model, while it would take only 12 h using the MV model. The minimal model therefore not only reproduces important tissue-level electrophysiological properties, but also is the fastest to compute, and therefore the most useful for large-scale 3D simulations in realistic anatomies. In particular, the MV model is very useful for pioneering studies, as in previous cases where the effects of fiber anisotropy on reentry destabilization (Fenton and Karma, 1998) and stabilizing electrotonic effects (Cherry and Fenton, 2004) were discovered first using a minimal model, and verified subsequently using more complex models (Rappel, 2001; Ten Tusscher and Panfilov, 2006a).

Another approach to improving computational efficiency was developed by Bernus et al. (2002b, 2003), where the upstroke dynamics are slowed down to allow for a decrease in spatial and temporal resolution, thereby decreasing computational demand. While this approach can produce substantial savings, it also can alter certain model properties, specifically the AP upstroke morphology and amplitude and potentially spiral wave trajectories. This method can be useful for many 2D and 3D simulations; however, its main limitation is that its dependence on decreasing the spatial resolution may not allow its use when it is necessary to include realistic small-scale ventricular architecture, including abrupt changes in fiber orientation, pectinate muscles, and tissue heterogeneities such as blood vessels.

4.7. *Transmural heterogeneity*

The minimal model accurately reproduces available data on differences in APD rate dependence, upstroke velocity, AP amplitude, and AP morphology among human endocardial, epicardial, and midmyocardial cells. In contrast to canine ventricular myocardium (Gussak and Antzelevitch, 2003), human endocardial cells have the shortest APs (Drouin et al., 1995, 1998; Li et al., 1998, Pereon et al., 2000), a difference reproduced by the minimal model. On the other hand, epicardial cells in the TNNP model have slightly shorter APDs than endocardial cells. In addition, our model indicates a greater difference in APD of the midmyocardial cells at longer DIs (about 150 ms), with this difference decreasing as the DI is decreased. The TNNP model has a much smaller difference of about 50 ms at long DIs, and the BWZVP model, which also has parameter variations for epicardial, endocardial, and midmyocardial cells, has no difference in APD between epicardial and endocardial cells and a difference of only about 40 ms with respect to midmyocardial cells. The longer APD of midmyocardial cells is one proposed explanation for the origin of the T-wave on the ECG (Gima and Rudy, 2002; Gussak and Antzelevitch, 2003), and in support of this hypothesis, our model produces a more pronounced T-wave than the TNNP model when calculated using a region of the left ventricular wall containing epicardial, endocardial, and midmyocardial cells.

4.8. *Using the minimal model to reproduce experimental and simulated data*

As has been shown, the minimal model is able to reproduce a range of properties exhibited experimentally or by other models (see Table 2 and Figs. 1, 8 and 11). Because the number of parameters involved is significantly smaller than for other models, it is possible to understand the role each parameter plays in producing properties like APD and CV restitution. Therefore, it is substantially easier to obtain fittings for different data sets. In this paper, we have shown fittings both to experimental APD and CV restitution data and AP morphologies for three types of human ventricular cells as well as fittings of the PB and TNNP models that reproduce not only their APD and CV restitution curves, but also their 2D reentry dynamics. The model can be adapted easily to account for external stimulation during defibrillation (Puwal and Roth, 2006) and to reproduce ion channelopathies such as Brugada Syndrome (Fenton et al., 2004).

4.9. *Limitations*

Although the minimal model has many benefits for tissue-level studies, it has certain limitations as well. While the model fits experimental data points well, the available APD restitution data for midmyocardial cells is fairly sparse. Additional experiments may reveal a different restitution curve shape than what has been fitted to the available data. In some cases, values from the literature used in developing the model fittings actually vary quite substantially. The lack of agreement in establishing these values affects the accuracy with which the model can reflect the actual physiology.

The 3D implementation of epicardial, endocardial, and midmyocardial cell distribution shown here is a straightforward assignment based on each cell type occupying a specific fraction

Please cite this article as: Bueno-Orovio, A., et al., Minimal model for human ventricular action potentials in tissue. J. Theor. Biol. (2008), doi:10.1016/j.jtbi.2008.03.029

of the tissue thickness. The distribution of epicardial, endocardial, and midmyocardial cells within the human ventricular wall is an area of active study and is likely more complicated than the straightforward distinct layers implemented here (Nash et al., 2006). In addition, only transmural gradients in AP properties were included. Other types of heterogeneity, including apicobasal, left–right, and anterior–posterior gradients, have not yet been incorporated into the minimal model.

4.10. Conclusions

We have presented a MV model that reproduces important properties of human ventricular epicardial, endocardial, and midmyocardial tissue, including resting membrane potential, threshold for excitation, maximum upstroke velocity, AP morphology, APD and CV restitution curves, and the minimum values of APD, DI, and CV required for propagation. The model was not developed as an adiabatic reduction of other more detailed models (Bernus et al., 2002a; Ten Tusscher and Panfilov, 2006b), but instead is constructed to reproduce total fast inward, slow inward, and slow outward currents. The main advantages of this model, with its unique formulation, are that its small number of parameters facilitates understanding the role of each individual parameter in determining the dynamics, and that its streamlined form makes the process of fitting the model to data obtained from experiments (whether from tissue that is normal, diseased, or exposed to pharmacological agents) or from other models faster and more straightforward.

Although biophysically detailed models are necessary to study certain types of phenomena, including the roles of concentration changes and particular ionic currents, their complexity can give rise to very serious limitations. In particular, the overall complexity of detailed models leads to uncertainty in developing equations and fitting their parameters. The large number of variables, parameters, and equations creates a huge parameter space, with the number of local minima increasing with the complexity of the model. Therefore, finding the true global minimum requires as many parameter restrictions as possible by including all possible experimental dynamics. Since this is not feasible, the local minimum corresponding to the best fit to the data may not be obtainable. Consequently, while the model may reproduce the data used to fit it, it may produce unrealistic results when tested in other regimes. This can limit the model's applicability to only a certain window of physiological conditions. For example, complex models are not always tested at fast pacing rates and therefore may develop problems when subjected to rates encountered during tachyarrhythmias (Fenton and Cherry, 2007). As a result, for example, the Nygren et al. human atrial model (Nygren et al., 1998) produces delayed after depolarizations at fast rates (Cherry et al., 2008), the Pandit et al. rat ventricular model (Pandit et al., 2001) can reach a second stationary state at a depolarized voltage of -10 mV, and the TNNP model produces stable spiral waves when initiated with initial conditions of pacing at a BCL of 1 s, but produces breakup when initiated with initial conditions of pacing at a CL of 300 ms. Other models, including the DiFrancesco-Noble (1985) Purkinje, Winslow et al. (1999) canine ventricular, Luo–Rudy dynamic (Faber and Rudy, 2000) guinea pig ventricular, and Shannon et al. (2004) rabbit ventricular models, do not produce alternans at fast rates, despite alternans having been observed experimentally in these systems. Furthermore, because of the complex nature of these models, most when published show simulations performed only in single cells and not in tissue, so that it is not possible to know whether the model behaves properly in tissue. For instance, the Hund–Rudy canine ventricular model (Hund and Rudy, 2004), which reproduces in detail many characteristics of single cells, exhibits vastly different behavior in tissue because of electrotonic loading effects that alter activation of the L-type Ca^{2+} current (Cherry and Fenton, 2007), and the IMW model, as shown here, produces an unrealistically broad spread of frequencies spanning beyond the clinical values of tachycardia and fibrillation at the same time. These issues are also related to the intense computational demands of these models, which limit the analysis that can be performed, especially in realistic cardiac anatomies at a spatial resolution sufficient to prevent computational artifacts.

Furthermore, even with the optimal model fitting, an imprecise understanding or representation of the underlying biophysical processes may result in behavior that would not be seen experimentally or may prevent observed phenomena from being replicated. In addition, the computational demands of such models may prevent much of the range of their behavior from being known. Thus, while complex models remain important tools to address certain types of questions, minimal models like the one presented here can be useful in a number of situations where the use of more biophysically detailed models would be difficult, computationally prohibitive, or otherwise impractical.

Acknowledgements

This work was supported in part by the National Institutes of Health under Grant no. R01 HL075515-S03,-S04, the National Science Foundation under Grant nos. MRI-0320865 and PHY05-51164, and the Consejería de Educaión y Ciencia of the Junta de Comunidades de Castilla-La Mancha under Ph.D. Grant no. 03-056. The above research was facilitated through an allocation of advanced computing resources at the Pittsburgh Supercomputing Center, through the support of the National Science Foundation. We thank Robert F. Gilmour, Jr., Ronald Wilders, Olivier Bernus, and Victor Perez Garcia for useful discussions.

Role of the funding source

The funding sources played no role in the study design; in the collection, analysis, and interpretation of data; in the writing of the report; and in the decision to submit the paper for publication.

Appendix A

A.1. Derivation of the diffusion coefficient

The diffusion coefficient used in all tissue simulations was calculated specifically to represent the surface-to-volume ratio, capacitance, and surface area of human ventricular cells. From the cable equation analysis one obtains that the diffusion coefficient D is given by $D = 1/(S_V \rho C_m / A)$, where S_V is the surface-to-volume ratio, ρ is the cytoplasm resistivity, C_m is the membrane capacitance, and A is the surface area. We used the following values: $148.3 \pm 8.8\,\mu$m as an average length for a human ventricular cell (Li et al., 1999), $18.5 \pm 1.2\,\mu$m as an average diameter (Li et al., 1999), $C_m = 179 \pm 10$ pF (Li et al., 1999), and $\rho = 180 \pm 34\,\Omega$ cm (Lieberman et al., 1975). Considering a cylindrical cell approximation, these values result in a human ventricular diffusion coefficient of $D = 1.171 \pm 0.221\,\text{cm}^2/\text{s}$. All simulations were performed using this value, except as noted.

Please cite this article as: Bueno-Orovio, A., et al., Minimal model for human ventricular action potentials in tissue. J. Theor. Biol. (2008), doi:10.1016/j.jtbi.2008.03.029

A.2. Links to interactive Java applets and movies

Java applets are available for each of the five models. In each applet, the user can plot APs as well as transmembrane currents, ionic concentrations, and key gating variables for user-specified CLs.

PB model:	http://thevirtualheart.org/java/pb/pb0d.html
BWZVP model:	http://thevirtualheart.org/java/rpb/rpb0d.html
TNNP model:	http://thevirtualheart.org/java/tnnp/k0d.html
IMW model:	http://thevirtualheart.org/java/iyer/iyeretal0d.html
MV model:	http://thevirtualheart.org/java/4v/fourv0d.html

Movies of the spiral wave dynamics of the models are available (Fenton and Cherry, 2007) at http://www.scholarpedia.org/article/Models_of_cardiac_cell.

A.3. Sample parameter fitting code

This example code illustrates how to use Matlab in conjunction with the Optimization Toolbox to perform an automatic selection of parameter values for the minimal model. The necessary files can be obtained at http://thevirtualheart.org/fitter.tar.

References

Bernus, O., Wilders, R., Zemlin, C.W., Verschelde, H., Panfilov, A.V., 2002a. A computationally efficient electrophysiological model of human ventricular cells. Am. J. Physiol. 282, H2296–H2308.

Bernus, O., Verschelde, H., Panfilov, A.V., 2002b. Modified ionic models of cardiac tissue for efficient large scale computations. Phys. Med. Biol. 47, 1947–1959.

Bernus, O., Verschelde, H., Panfilov, A.V., 2003. Reentry in an anatomical model of the human ventricles. Int. J. Bifurcat. Chaos 13, 3693–3702.

Bueno-Orovio, A., Perez-Garcia, V.M., Fenton, F.H., 2006. Spectral methods for partial differential equations in irregular domains: the spectral smoothed boundary method. SIAM J. Sci. Comput. 28, 886–900.

Cherry, E.M., Fenton, F.H., 2004. Suppression of alternans and conduction blocks despite steep APD restitution: electrotonic, memory, and conduction velocity restitution effects. Am. J. Physiol. 286, H2332–H2341.

Cherry, E.M., Fenton, F.H., 2007. A tale of two dogs: analyzing two models of canine ventricular electrophysiology. Am. J. Physiol. 292, H43–H55.

Cherry, E.M., Hastings, H.M., Evans, S.J., 2008. Dynamics of human atrial cell models: restitution, memory, and intracellular calcium dynamics in single cells. Prog. Biophys. Mol. Biol., in press.

Clayton, R.H., Holden, A.V., 2002. Computational framework for simulating the mechanisms and ECG of re-entrant ventricular fibrillation. Physiol. Meas. 23, 707–726.

DiFrancesco, D., Noble, D., 1985. A model of cardiac electrical activity incorporating ionic pumps and concentration changes. Philos. Trans. R. Soc. London 307, 353–398.

Drouin, E., Charpentier, F., Gauthier, C., Laurent, K., LeMarec, H., 1995. Electrophysiologic characteristics of cells spanning the left ventricular wall of human heart: evidence for presence of M cells. J. Am. Coll. Cardiol. 26, 185–192.

Drouin, E., Lande, G., Charpentier, F., 1998. Amiodarone reduces transmural heterogeneity of repolarization in the human heart. J. Am. Coll. Cardiol. 32, 1063–1067.

Faber, G.M., Rudy, Y., 2000. Action potential and contractility changes in $[Na^+]_i$ overloaded cardiac myocytes: a simulation study. Biophys. J. 78, 2392–2404.

Fenton, F., 2000. Numerical simulations of cardiac dynamics. What can we learn from simple and complex models? Comput. Cardiol. (IEEE) 27, 251–254.

Fenton, F., Karma, A., 1998. Vortex dynamics in 3D continuous myocardium with fiber rotation: filament instability and fibrillation. Chaos 8, 20–47.

Fenton, F., Evans, S., Hastings, H., 1999. Memory in an excitable medium; a mechanism for spiral wave breakup in the low-excitability limit. Phys. Rev. Lett. 83, 3964–3967.

Fenton, F.H., 1999. Theoretical investigation of spiral and scroll wave instabilities underlying cardiac fibrillation. Ph.D. Thesis, Northeastern University, Boston, MA.

Fenton, F.H., Cherry, E.M., 2007. Models of cardiac cells. Scholarpedia.

Fenton, F.H., Cherry, E.M., Hastings, H.M., Evans, S.J., 2002a. Multiple mechanisms of spiral wave breakup in a model of cardiac electrical activity. Chaos 12, 852–892.

Fenton, F.H., Cherry, E.M., Banville, I., Gray, R.A., Hastings, H.M., Evans, S.J., 2002b. Validation of realistic 3d computer models of ventricular arrhythmias with optical mapping experiments. Pacing Clin. Electrophysiol. 24 (Part II), 538.

Fenton, F.H., Bueno Orovio, A., Cherry, E.M., Evans, S.J., 2004. Basis for the induction of phase two reentry in the Brugada syndrome: insights from computer simulations. Heart Rhythm 1, S224–S225.

Fenton, F.H., Cherry, E.M., Karma, A., Rappel, W.J., 2005. Modeling wave propagation in realistic heart geometries using the phase-field method. Chaos 15, 013502.

Fink, M., Giles, W., Noble, D., 2006. Potassium currents and repolarization reserve in mathematical models of human ventricle. Philos. Trans. R. Soc. A 364, 1207–1222.

Fletcher, R., 1987. Practical Methods of Optimization. Wiley, New York.

Gill, P.E., Murray, W., Wright, M.H., 1981. Practical Optimization. Academic Press, London.

Gima, K., Rudy, Y., 2002. Ionic current basis of electrocardiographic waveforms: a model study. Circ. Res. 90, 889–896.

Girouard, S.D., Pastore, J.M., Laurita, K.R., Greogry, K.W., Rosenbaum, D.S., 1996. Optical mapping in a new guinea pig model of ventricular tachycardia reveals mechanisms for multiple wavelengths in a single reentrant circuit. Circulation 93, 603–613.

Gussak, I., Antzelevitch, C. (Eds.), 2003. Cardiac Repolarization: Bridging Basic and Clinical Science. Humana, Totowa, NJ.

Henry, H., Rappel, W.J., 2005. Dynamics of conduction blocks in a model of paced cardiac tissue. Phys. Rev. E 71, 051911.

Hund, T.J., Rudy, Y., 2004. Rate dependence and regulation of action potential and calcium transient in a canine cardiac ventricular cell model. Circulation 110, 3168–3174.

Hund, T.J., Kucera, J.P., Otani, N.F., Rudy, Y., 2001. Ionic charge conservation and long-term steady state in the Luo–Rudy dynamic cell model. Biophys. J. 81, 3324–3331.

Iost, N., Virag, L., Opincairiu, M., Szecsi, J., Varro, A., Papp, J.G., 1998. Delayed rectifier potassium current in undiseased human ventricular myocytes. Cardiovasc. Res. 40, 508–515.

Iyer, V., Mazhari, R., Winslow, R.L., 2004. A computational model of the human left-ventricular epicardial myocytes. Biophys. J. 87, 1507–1525.

Kneller, J., Ramirez, R.J., Chartier, D., Courtemanche, M., Nattel, S., 2002. Time-dependent transients in an ionically based mathematical model of the canine atrial action potential. Am. J. Physiol. 282, H1437–H1451.

Koller, M.L., Maier, S.K., Gelzer, A.R., Bauer, W.R., Meesman, M., Gilmour Jr., R.F., 2005. Altered dynamics of action potential restitution and alternans in humans with structural heart disease. Circulation 112, 1542–1548.

Li, G.R., Feng, J., Yue, L., Carrier, M., 1998. Transmural heterogeneity of action potentials and I_{to1} in myocytes isolated from the human right ventricle. Am. J. Physiol. 275, H369–H377.

Li, G.R., Yang, B., Feng, J., Bosch, R.F., Carrier, M., Nattel, S., 1999. Transmembrane I_{Ca} contributes to rate-dependent changes of action potentials in human ventricular myocytes. Am. J. Physiol. 276, H98–H106.

Lieberman, M., Sawanobori, T., Kootsey, J.M., Johnson, E.A., 1975. A synthetic strand of cardiac muscle: its passive electrical properties. J. Gen. Physiol. 65, 527–550.

Morgan, J.M., Cunningham, D., Rowland, E., 1992. Dispersion of monophasic action potential duration: demonstrable in humans after premature ventricular extrastimulation but not in steady state. J. Am. Coll. Cardiol. 19, 1244–1253.

Nabauer, M., Beuckelmann, D.J., Uberfuhr, P., Steinbeck, G., 1996. Regional differences in current density and rate-dependent properties of the transient outward current in subepicardial and subendocardial myocytes of human left ventricle. Circulation 93, 169–177.

Nanthakumar, K., Jalife, J., Masse, S., Downar, E., Pop, M., Asta, J., Ross, H., Rao, V., Mironov, S.F., Sevaptsidis, E., Rogers, J.M., Wright, G., Dhopeshwarkar, R., 2007. Optical mapping of Langendorff perfused human hearts: establishing a model for the study of ventricular fibrillation in humans. Am. J. Physiol. 293, H875–H880.

Nash, M.P., Panfilov, A.V., 2004. Electromechanical model of excitable tissue to study reentrant cardiac arrhythmias. Prog. Biophys. Mol. Biol. 85, 501–522.

Nash, M.P., Bradley, C.P., Sutton, P.M., Clayton, R.H., Kallis, P., Hayward, M.P., Peterson, D.J., Taggart, P., 2006. Whole heart action potential duration restitution properties in cardiac patients: a combined clinical and modeling study. Exp. Physiol. 91, 339–354.

Nygren, A., Fiset, C., Firek, L., Clark, J.W., Lindblad, D.S., Clark, R.B., Giles, W.R., 1998. Mathematical model of an adult human atrial cell: the role of K^+ currents in repolarization. Circ. Res. 82, 63–81.

Oliver, R.A., Krassowska, W., 2005. Reproducing cardiac restitution properties using the Fenton–Karma membrane model. Ann. Biomed. Eng. 33, 907–911.

Pak, H.N., Hong, S.J., Hwang, G.S., Lee, H.S., Park, S.W., Ahn, J.C., Moo Ro, Y., Kim, Y.H., 2004. Spatial dispersion of action potential duration restitution kinetics is associated with induction of ventricular tachycardia/fibrillation in humans. J. Cardiovasc. Electrophysiol. 15, 1357–1363.

Pandit, S.V., Clark, R.B., Giles, W.R., Demir, S.S., 2001. A mathematical model of action potential heterogeneity in adult rat left ventricular myocytes. Biophys. J. 81, 3029–3051.

Peeters, G.A., Sanguinetti, M.C., Eki, Y., Konarzewska, H., Renlund, D.G., Karwande, S.V., Barry, W.H., 1995. Method for isolation of human ventricular myocytes from single endocardial and epicardial biopsies. Am. J. Physiol. 268, H1757–H1764.

Pereon, Y., Demolombe, S., Baro, I., Drouin, E., Charpentier, F., Escande, D., 2000. Differential expression of KvLQT1 isoforms across the human ventricular wall. Am. J. Physiol. 278, H1908–H1915.

Priebe, L., Beuckelmann, D.J., 1998. Simulation study of cellular electric properties in heart failure. Circ. Res. 82, 1206–1223.

Puwal, S., Roth, B.J., 2006. Numerical simulations of synchronized pacing. J. Biol. Syst. 14, 101–112.

Please cite this article as: Bueno-Orovio, A., et al., Minimal model for human ventricular action potentials in tissue. J. Theor. Biol. (2008), doi:10.1016/j.jtbi.2008.03.029

Qu, Z., Garfinkel, A., Chen, P.S., Weiss, J.N., 2000. Mechanisms of discordant alternans and induction of reentry in simulated cardiac tissue. Circulation 102, 1664–1670.

Rappel, W.J., 2001. Filament instability and rotational tissue anisotropy: a numerical study using detailed cardiac models. Chaos 11, 71–80.

Reuter, H., 1984. Ion channels in cardiac cell membranes. Annu. Rev. Physiol. 46, 473–484.

Rush, S., Larsen, H., 1978. A practical algorithm for solving dynamic membrane equations. IEEE Trans. Biomed. Eng. 25, 389–392.

Sakakibara, Y., Furukawa, T., Singer, D.H., Jia, H., Backer, C.L., Arentzen, C.E., Wasserstrom, J.A., 1993. Sodium current in isolated human ventricular myocytes. Am. J. Physiol. 265, H1301–H1309.

Saumarez, R.C., Camm, A.J., Panagos, A., Gill, J.S., Stewart, J.T., de Belder, M.A., Simpson, I.A., McKenna, W.J., 1992. Ventricular fibrillation in hypertrophic cardiomyopathy is associated with increased fractionation of paced right ventricular electrograms. Circulation 86, 467–474.

Saumarez, R.C., Heald, S., Gill, J., Slade, A.K.B., de Belder, M., Walczak, F., Rowland, E., Ward, D.E., Camm, A.J., 1995. Primary ventricular fibrillation is associated with increased paced right ventricular electrogram fractionation. Circulation 92, 2565–2571.

Shannon, T.R., Wang, F., Puglisi, J., Weber, C., Bers, D.M., 2004. A mathematical treatment of integrated Ca dynamics within the ventricular myocytes. Biophys. J. 87, 3351–3371.

Stevens, C., Remme, E., LeGrice, I., Hunter, P., 2003. Ventricular mechanics in diastole: material parameter sensitivity. J. Biomech. 36, 737–748.

Syed, Z., Vigmond, E., Leon, L.J., 2005. Atrial cell action potential parameter fitting using genetic algorithms. Med. Biol. Eng. Comput. 43, 561–571.

Taggart, P., Sutton, P.M., Opthof, T., Coronel, R., Trimlett, R., Pugsley, W., Kallis, P., 2000. Inhomogeneous transmural conduction during early ischemia in patients with coronary artery disease. J. Mol. Cell Cardiol. 32, 621–639.

Ten Tusscher, K.H., Panfilov, A.V., 2006a. Alternans and spiral breakup in a human ventricular tissue model. Am. J. Physiol. 29, H1088–H1100.

Ten Tusscher, K.H., Panfilov, A.V., 2006b. Cell model for efficient simulation of wave propagation in human ventricular tissue under normal and pathological conditions. Phys. Med. Biol. 51, 6141–6156.

Ten Tusscher, K.H., Noble, D., Noble, P.J., Panfilov, A.V., 2004. A model for human ventricular tissue. Am. J. Physiol. 286, H1573–H1589.

Ten Tusscher, K.H., Bernus, O., Hren, R., Panfilov, A.V., 2006. Comparison of electrophysiological models for human ventricular cells and tissue. Prog. Biophys. Mol. Biol. 90, 326–345.

Vigmond, E.J., Leon, L.J., 2002. Restitution curves and the stability of reentry in three-dimensional simulations of cardiac tissue. Comput. Vis. Sci. 4, 237–247.

Watanabe, M.A., Fenton, F.H., Evans, S.J., Hastings, H.M., Karma, A., 2001. Mechanisms for discordant alternans. J. Cardiovasc. Electrophysiol. 12, 196–206.

Winslow, R.L., Rice, J., Jafri, S., Marban, E., O'Rourke, B., 1999. Mechanisms of altered excitation–contraction coupling in canine tachycardia-induced heart failure. II. Model studies. Circ. Res. 84, 571–586.

Yue, A.M., Franz, M.R., Roberts, P.R., Morgan, J.M., 2005. Global endocardial electrical restitution in human right and left ventricles determined by noncontact mapping. J. Am. Coll. Cardiol. 46, 1067–1075.

Please cite this article as: Bueno-Orovio, A., et al., Minimal model for human ventricular action potentials in tissue. J. Theor. Biol. (2008), doi:10.1016/j.jtbi.2008.03.029